RESEARCH ARTICLE

Prediction of DNA Repair Inhibitor Response in Short-Term Patient-Derived Ovarian Cancer Organoids

Sarah J. Hill[1,2], Brennan Decker[2], Emma A. Roberts[1], Neil S. Horowitz[3], Michael G. Muto[3], Michael J. Worley Jr[3], Colleen M. Feltmate[3], Marisa R. Nucci[2], Elizabeth M. Swisher[4,5], Huy Nguyen[1,6], Chunyu Yang[1], Ryuji Morizane[7], Bose S. Kochupurakkal[6], Khanh T. Do[8], Panagiotis A. Konstantinopoulos[9], Joyce F. Liu[9,10], Joseph V. Bonventre[7], Ursula A. Matulonis[9,10], Geoffrey I. Shapiro[6,8,10], Ross S. Berkowitz[3], Christopher P. Crum[2], and Alan D. D'Andrea[1,6]

ABSTRACT Based on genomic analysis, 50% of high-grade serous ovarian cancers (HGSC) are predicted to have DNA repair defects. Whether this substantial subset of HGSCs actually have functional repair defects remains unknown. Here, we devise a platform for functional profiling of DNA repair in short-term patient-derived HGSC organoids. We tested 33 organoid cultures derived from 22 patients with HGSC for defects in homologous recombination (HR) and replication fork protection. Regardless of DNA repair gene mutational status, a functional defect in HR in the organoids correlated with PARP inhibitor sensitivity. A functional defect in replication fork protection correlated with carboplatin and CHK1 and ATR inhibitor sensitivity. Our results indicate that a combination of genomic analysis and functional testing of organoids allows for the identification of targetable DNA damage repair defects. Larger numbers of patient-derived organoids must be analyzed to determine whether these assays can reproducibly predict patient response in the clinic.

SIGNIFICANCE: Patient-derived ovarian tumor organoids grow rapidly and match the tumors from which they are derived, both genetically and functionally. These organoids can be used for DNA repair profiling and therapeutic sensitivity testing and provide a rapid means of assessing targetable defects in the parent tumor, offering more suitable treatment options. *Cancer Discov; 8(11); 1404–21. ©2018 AACR.*

INTRODUCTION

Ovarian cancer represents the fifth leading cause of cancer death in women in the United States (1). The major epithelial subtypes are serous, mucinous, endometrioid, and clear cell (2). The serous subtype comprises approximately 60% of ovarian tumors (3), and high-grade serous ovarian cancers (HGSC), which include those arising in *BRCA1* or *BRCA2* mutation carriers (2), are the most lethal. Almost 80% of patients with HGSC succumb to their disease (3). Limited therapeutic options and a lack of biomarkers predicting treatment response contribute to this poor survival.

Genomic, transcriptomic, methylation, and pathway analyses reveal that up to 50% of HGSCs harbor alterations in DNA damage response genes or pathways (4), potentially leading to a DNA repair defect. Consequently, there has been a focus on therapies targeting repair defects in HGSC (5). The initial treatment of patients with HGSC is formulaic and relies on platinum-based agents that create DNA cross-links, leading to replication and transcription arrest in the tumor cells (3, 6). Patients initially receive a combination of paclitaxel and a platinum agent (either neoadjuvant, post-cytoreduction, or both) and undergo cytoreductive surgery. However, there is currently no means of determining whether a patient's tumor will be platinum-sensitive (3). Most patients initially respond well to a platinum-based regimen, although there is a subset of patients whose cancers are platinum-refractory at the outset. These patients may benefit from different initial therapies or combination therapies. Even for those patients who initially respond, platinum resistance can develop with limited effective additional therapies available (3).

PARP inhibitors (PARPi) exert their cytotoxic effects through a synthetic lethal pathway, thereby killing tumor cells with defects in homologous recombination (HR) and/or in the protection of stalled replication forks (7). *BRCA1* and *BRCA2* (*BRCA1/2*)–associated HGSCs, and a subset of sporadic HGSCs, often respond to PARPis (7). However, there are no reliable tests for predicting which tumors will respond to these agents and defining the nature of the underlying functional defect that leads to the response (8, 9). Patients with tumors harboring *BRCA1/2* mutations who initially respond to PARPis eventually develop drug resistance through multiple mechanisms, including somatic reversion mutations in *BRCA1/2*, epigenetic reversion of *BRCA1/2* promoter methylation, overexpression of a *BRCA1/2* hypomorph, loss of PARP1 expression, initiation of drug efflux, or acquisition of new mutations in or silencing of other DNA damage repair genes such as *REV7*, *EZH2*, and *TP53BP1* (7, 10, 11). These mechanisms may lead to restoration of either HR activity or protection of stalled replication forks (12).

New classes of drugs, including ATR and CHK1 inhibitors, may be useful for the treatment of PARPi-resistant tumors (12, 13). The specific mechanism of PARPi resistance

[1]Department of Radiation Oncology, Dana-Farber Cancer Institute, Harvard Medical School, Boston, Massachusetts. [2]Department of Pathology, Brigham and Women's Hospital, Harvard Medical School, Boston, Massachusetts. [3]Division of Gynecologic Oncology, Department of Obstetrics, Gynecology and Reproductive Biology, Brigham and Women's Hospital, Harvard Medical School, Boston, Massachusetts; Dana-Farber Cancer Institute, Boston, Massachusetts. [4]Division of Gynecologic Oncology, University of Washington, Seattle, Washington. [5]Division of Medical Genetics, Department of Medicine, University of Washington, Seattle, Washington. [6]Center for DNA Damage and Repair, Dana-Farber Cancer Institute, Boston, Massachusetts. [7]Renal Division, Brigham and Women's Hospital, Boston, Massachusetts; Department of Medicine, Harvard Medical School, Boston, Massachusetts; Harvard Stem Cell Institute, Cambridge, Massachusetts. [8]Early Drug Development Center, Department of Medical Oncology, Dana-Farber Cancer Institute, Boston, Massachusetts. [9]Department of Medical Oncology, Dana-Farber Cancer Institute, Harvard Medical School, Boston, Massachusetts. [10]Department of Medicine, Brigham and Women's Hospital, Boston, Massachusetts.

Note: Supplementary data for this article are available at Cancer Discovery Online (http://cancerdiscovery.aacrjournals.org/).

Corresponding Author: Alan D. D'Andrea, Dana-Farber Cancer Institute, HIM 243, 450 Brookline Avenue, Boston, MA 02215. Phone: 617-632-2112; Fax: 617-632-6069; E-mail: Alan_Dandrea@dfci.harvard.edu

doi: 10.1158/2159-8290.CD-18-0474

(i.e., restoration of HR or functional correction of defects in replication fork protection) may determine the efficacy of these agents in either *BRCA1/2*-mutant or sporadic HGSC. A better understanding of the functional defects in HGSCs is needed to understand which therapies are best suited for each molecular defect and which combinations are least likely to select for resistance.

Functional assays dissecting the specific DNA damage repair defects in a tumor are useful for assessing specific targets for each patient. Organoid cultures of patient-derived tumors provide an easily manipulable and inexpensive model system for these functional assays. Organoids are derived from human stem and/or primary tumor cells that organize into three-dimensional structures anatomically and functionally mimicking the tumor from which they are derived. To date, organoids have been generated from primary prostate, colon, and pancreatic tumors, among others (14–19).

Organoids are faster, easier, and less expensive to generate than patient-derived xenograft (PDX) models in mice. Additionally, organoids uncover clonal heterogeneity of tumors and can be generated without long periods of *ex vivo* selection. Furthermore, organoid cultures contain immune cells representative of the tumor immune microenvironment (Hill and colleagues, unpublished; and Jenkins and colleagues, ref. 20) which, unlike PDX models, may enable the testing of immune-checkpoint blockade or other immunotherapies. Overall, organoids are potentially faithful tumor models that allow for functional testing, prediction of therapeutic sensitivity, and interrogation of specific biomarkers (14–21). Large-scale studies of organoids, with comparison with patient outcomes, will be required to prove the utility of this model system in the clinic (18, 19, 21).

We reasoned that patient-derived HGSC organoids would be an ideal model system for measuring DNA repair activity and for determining which repair defects confer sensitivity to a variety of DNA repair drugs or drug combinations. We have generated a platform of assays to query the function of the key BRCA/Fanconi anemia DNA damage repair mechanisms, such as HR and stalled fork protection, and have applied these assays to HGSC organoid cultures. We used these data, along with genomic assessment of the organoids and tumors from which they were derived, to evaluate which molecular defects confer therapeutic sensitivities. We determined that genomic data alone cannot accurately predict the true DNA repair capacity of HGSCs and that a rapid functional platform is needed for targeted drug selection.

RESULTS

Patient-Derived HGSC Organoid Cultures Morphologically and Molecularly Match the Parent Tumors from Which They Were Derived

Short-term organoid cultures were generated from 22 patients with HGSC and 1 patient with low-grade serous carcinoma (LGSC). One HGSC patient had a carcinosarcoma, with a high-grade serous epithelial component and a spindle-cell mesenchymal component. Organoids were derived primarily from solid tumors extracted from primary, metastatic, or recurrent tumor sites (Fig. 1A and B). Although we achieved a nearly 100% success rate in generating organoids from ascitic or pleural fluid, we favored the analysis of solid tumors because cells cultured from ascitic and pleural fluid may not accurately reflect the intrinsic biological features of a patient's tumor, such as drug accessibility or the local solid tumor microenvironment (22). Cases were collected over a period of 12 months and included samples from 17 patients with sporadic cancer and 6 patients with known *BRCA* pathway mutations (2 *BRCA1*-DF-17-39 and DF-17-107; 3 *BRCA2*-DF-17-115, DF-18-23, and DF-18-30; and 1 *RAD51C/FANCO*-DF-17-126; Fig. 1B). Fresh tumor tissue was digested to small multicellular units, and malignant cells were plated in Matrigel and growth factor–enriched media (Fig. 1A). Like other organoid cultures, our media required R-spondin 1, suggesting that the cultures were WNT-dependent (14). β-Estradiol was not required for culture maintenance. Organoids grew from single cells/cell clumps within 7 to 10 days of plating and were carried from 6 passages up to 30 passages (Fig. 1A). Thirty-four organoid lines (1–4 tumor sites per subject) were generated from the 23 patients (Fig. 1B).

Organoids were a morphologic and cytologic match for the parent tumors, based on hematoxylin and eosin (H&E) staining (Fig. 1C and E). Parent tumors and organoids displayed extensive nuclear pleomorphism, prominent nucleoli, and dense chromatin, thereby recapitulating all features of HGSCs.

IHC analysis of the organoids and parent tumors also matched. Most tumor–organoid pairs stained positive for the Müllerian marker PAX8, which is usually positive in HGSCs and LGSCs. The HGSC organoids examined exhibited a mutant staining pattern for the tumor suppressor p53, as is routinely present in HGSCs (Fig. 1C and E). The p53-mutant pattern ranged from pervasive dark staining, indicating overexpression of a mutant protein, to total loss of expression. Overall, the success rate for organoid generation was 80% to 90% in previously untreated HGSC cases, as well as in neoadjuvantly treated cases, provided there was grossly visible tumor at the time of debulking. Success rates in neoadjuvant cases declined if a patient had an extreme response to chemotherapy. Success rates in core biopsies varied, based on the percentage of viable tumor present.

We also analyzed one LGSC case that exhibited nuclear atypia and the characteristic wild-type p53 staining pattern in both the parent tumor and organoids (Supplementary Fig. S1A). We also successfully generated organoids from endometrioid and clear cell ovarian carcinoma, benign fallopian tube which cultures demonstrated characteristic ciliated cells of the parent tissue (Supplementary Fig. S1B), and borderline serous and gastrointestinal-type borderline mucinous tumors (Supplementary Fig. S1C).

For the 34 organoid cultures, the genomes of the organoids and corresponding tumors were also analyzed by whole-exome sequencing (WES). Somatic mutations were identified by comparing these sequences with the WES of the germline of each patient. Somatic mutations discovered in early passages (passages 1–2) of each organoid were compared with the corresponding tumor sample. Germline mutations were found in tumors and organoids from each of the 5 patients with known germline mutations in HR genes and in 1 patient who had not undergone germline testing (Fig. 1B). A median of 98.2% of mutations identified in the tumors were also

A

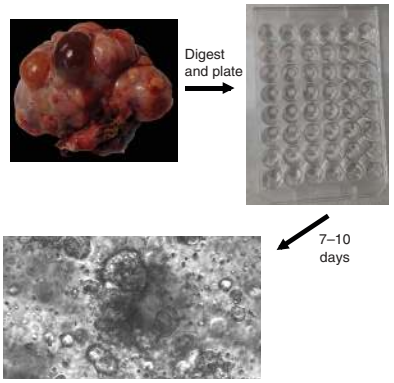

B

Patient	Treatment/histology	#Lines	Sites from which organoids generated	Germline	Copy number
DF-17-39	Recurrent/HGSC	4	Rectosigmoid mesentery, transverse colon mesentery, supracolic omentum mesentery, diaphragm nodules	*BRCA1*	*MYC* Amp
DF-17-103	Neoadjuvant/HGSC	1	Omentum		
DF-17-104	Neoadjuvant/HGSC	1	Omentum		
DF-17-107	Neoadjuvant/HGSC	3	Right ovary, left ovary, omentum	*BRCA1*	*MYC* Amp
DF-17-115	Untreated/HGSC	1	Left ovary	*BRCA2*	
DF-17-116	Neoadjuvant/HGSC	1	Omentum		
DF-17-121	Recurrent/HGSC	1	Pleural effusion		
DF-17-123	Untreated/HGSC	3	Right ovary, left ovary, omentum		*MYC* Amp
DF-17-126	Untreated/HGSC	1	Omentum	*RAD51C*	
DF-17-132	Untreated and post-neoadjuvant/HGSC	3	Untreated omentum, post-neoadjuvant omentum, and cecal mesentery		
DF-17-134	Untreated/HGSC	2	Left ovary, right ovary		
DF-18-1	Neoadjuvant/HGSC	1	Omentum		*CCNE1* Amp
DF-18-7	Untreated/HGSC	1	Right ovary		
DF-18-8	Untreated/HGSC	1	Colonic mesentery		*MYC* Amp
DF-18-12	Untreated/HGSC	1	Left ovary		*CCNE1* Amp
DF-18-17	Neoadjuvant/HGSC	1	Omentum		
DF-18-23	Neoadjuvant/HGSC	1	Right ovary	*BRCA2*	*MYC* Amp
DF-18-30	Untreated/ Carcinosarcoma	1	Left ovary	*BRCA2*	*MYC* Amp
DF-18-43	Neoadjuvant/HGSC	2	Omentum and left ovary		
DF-18-47	Untreated/HGSC	1	Omentum		*CCNE1* Amp
DF-18-48	Neoadjuvant/LGSC	1	Omentum		
DF-18-50	Neoadjuvant/HGSC	1	Omentum		*CCNE1* Amp
DF-18-54	Neoadjuvant/HGSC	1	Omentum		

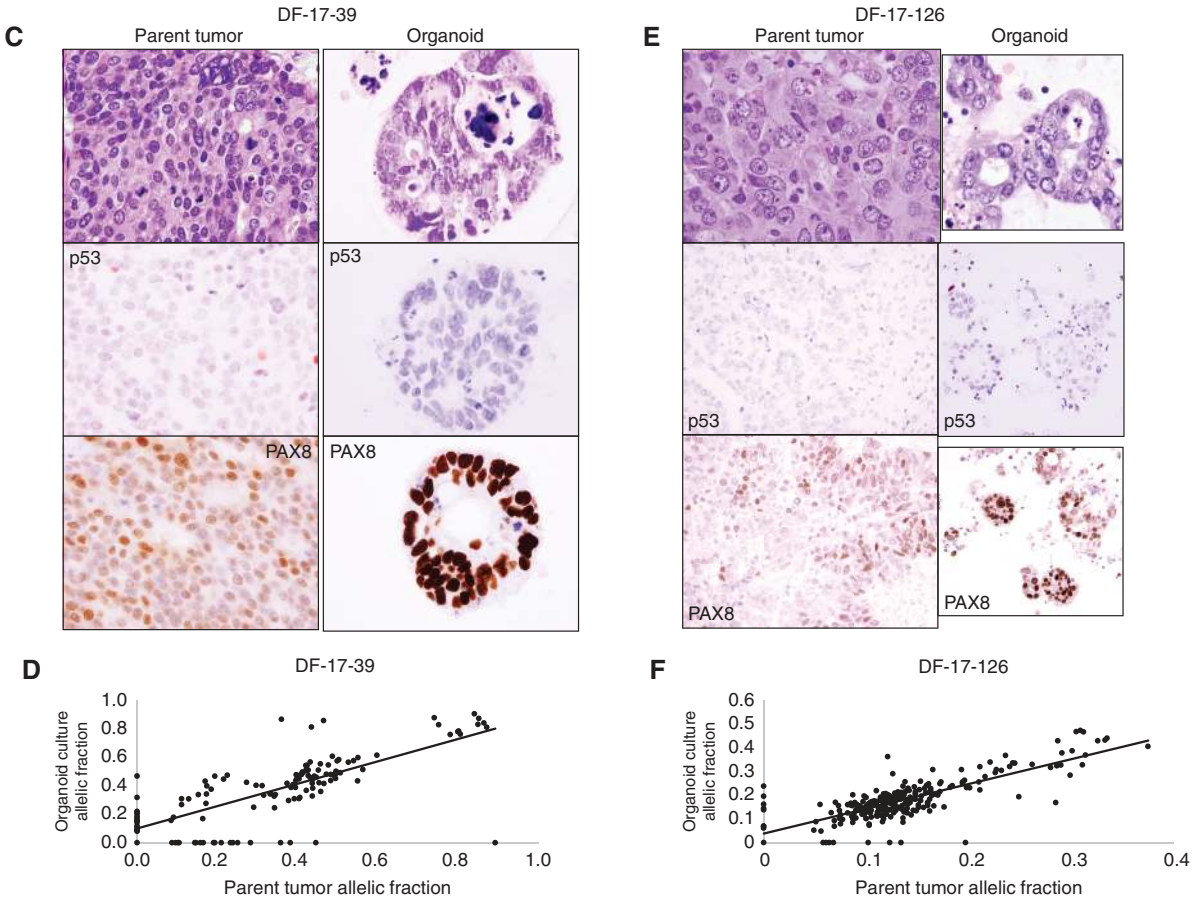

Figure 1. HGSC organoids morphologically and molecularly mimic the parent tumors from which they were derived. **A,** Illustration of organoid generation from tumor, to plating in Matrigel, to organoid growth (Brightfield image). **B,** Table of patient, treatment status at time of surgery where parent tumor was obtained, histology, number of lines established, tumor sites obtained for organoid generation, and known germline and copy-number status. **C** and **E,** Histologic comparison of two separate parent tumors (left) to the matched organoid cultures (right) by morphology (H&E, top), and p53 and PAX8 expression (bottom two plots) paired with molecular comparison (**D** and **F**) by analysis of mutant allele fractions of somatic mutations in the organoid versus parent tumors. **C** and **D** compare parent tumor and organoids generated from a rectosigmoid colon metastasis from a recurrent HGSC. **E** and **F** compare organoids and parent tumor from an omental metastasis of an untreated HGSC.

found in the matched organoid line (Supplementary Fig. S2; Supplementary Tables S1 and S2). Similarly, 98.8% of mutations found in the organoids were also present in the parent tumor (Supplementary Fig. S2; Supplementary Table S2). The overall copy number and allelic imbalance across the genome were also similar between organoids and parent tumors (Supplementary Fig. S3). The organoids were therefore a close representation of the somatic genetic composition of the parent tumor and did not acquire new somatic mutations during the short (7–10 day) *ex vivo* growth period. In all cases, the previously defined driver mutations of the parent tumors were retained in the organoids. Minor genetic differences between tumors and organoids likely represented sampling errors incurred during collection of tissue for DNA for sequencing or during organoid production. Furthermore, the relative abundance of somatic mutations (mutant allele fraction) was similar between tumors and organoids. Representative mutant allele fraction concordance plots are shown in Fig. 1D and F, illustrating a high level of similarity for two tumor–organoid pairs. The concordance plots (Supplementary Fig. S2), genome-wide copy-number status (Supplementary Fig. S3), and somatic variants (Supplementary Table S3) for all tumor–organoid pairs are shown. Taken together, the high level of multidimensional concordance between tumor and organoid culture indicates that short-term HGSC organoid cultures are a representative model of the parent tumors for assessing DNA damage repair defects.

Most HGSCs Exhibit Functional HR Repair

The HR capacity of the organoid cultures was assessed using multiple surrogate markers. First, all organoid cultures were tested for sensitivity to the PARPi olaparib (Fig. 2 and Table 1), because olaparib sensitivity is a useful surrogate marker for an HR defect (7). They were also tested for sensitivity to replication fork stalling agents, including carboplatin, as well as the CHK1 inhibitor prexasertib and the ATR inhibitor VE-822. These latter agents are known to induce replicative stress. A subset of organoid cultures were also tested for sensitivity to the replication stress (RS)–inducing nucleoside analogue gemcitabine and to the conventional HGSC agents doxorubicin and paclitaxel. To ensure that the drug concentrations applied to the organoids could kill ovarian cancer cells, these agents were initially tested in the OVCAR8 cell line transfected with a control or *BRCA1*-specific siRNA and shown to cause the expected dose-dependent cytotoxicity (Supplementary Fig. S4A and S4C). Sensitivity standards were established for each drug (Supplementary Fig. S5–S8), and the sensitivity results for all 34 lines are reported in Table 1.

Second, the ability of organoid tumor cells to assemble RAD51 foci, either pre- or post-irradiation (IR), was tested. In the process of HR, RAD51 is loaded onto the ends of a double-strand break (DSB), allowing the resected DSB to invade the sister chromatid (6). The assembly of RAD51 foci is a surrogate marker for the ability of a cell to perform HR, up to the stage of RAD51 loading (6). This assay does not measure HR steps downstream of RAD51 loading. Organoid cultures were treated with 0 or 10 Gy, prior to assaying for RAD51 foci (23). Organoids were costained for γH2AX to mark DNA damage and for geminin to mark cells in S phase (Fig. 2; ref. 23). Stained slides were examined first for geminin positivity and subsequently for RAD51 foci. The detection of 1 to 3 cells over multiple high-power fields with RAD51 foci was scored as positive, and the corresponding tumor was scored as HR competent (Fig. 2 and Table 1; ref. 23). For RAD51-positive organoids, RAD51 foci and extensive γH2AX nuclear positivity were detected both pre- and post-IR in most cases.

Organoids from 2 patients illustrate the utility of the HR functional assays (Fig. 2). Organoids were established from 4 tumor sites from a *BRCA1* mutation carrier whose tumor had acquired PARPi resistance (patient DF-17-39; Fig. 2A and B; Table 1). All organoids were olaparib-resistant, but sensitive to carboplatin, prexasertib, VE-822, and gemcitabine (Fig. 2A and Table 1). Interestingly, the functional results for this patient matched the clinical response. The patient was later treated with prexasertib and exhibited stable disease at sites from which organoids had been derived. Subsequent treatment with carboplatin and gemcitabine resulted in a decrease in disease burden for several months (Supplementary Table S4). The patient subsequently recurred and succumbed to her disease, suggesting acquired resistance to these agents. The organoids from all 4 sites exhibited RAD51 foci (Fig. 2B and Table 1), indicating HR competence, consistent with olaparib resistance. Despite PARPi resistance in the organoids and in the patient's tumor, these organoids remained carboplatin-sensitive, a surrogate marker for a defect in stalled replication fork protection. These results confirmed that the HR and fork repair functions of BRCA1 are independent (24, 25) and that the molecular mechanism of PARPi resistance restored HR but not stalled fork protection.

In contrast to patient DF-17-39, organoids generated from a patient carrying a *RAD51C/FANCO* germline mutation (DF-17-126) were sensitive to olaparib, suggesting an HR defect, and were also sensitive to carboplatin, prexasertib, VE-822, and gemcitabine (Fig. 2C). Consistent with this olaparib sensitivity, these organoids exhibited no RAD51 focus formation, demonstrating that the tumor was indeed HR deficient (Fig. 2D and Table 1).

Only 2 of 33 (6%) of the organoid cultures tested were olaparib-sensitive (Fig. 2 and Table 1), suggesting that organoids derived from most HGSCs do not have functional HR defects, despite their genetic findings, and predicting that the corresponding tumors will be insensitive to PARP inhibition. The overall rate of carboplatin, prexasertib, VE-822, and gemcitabine sensitivity was much higher (41%, 47%, 44%, and 82%, respectively) and did not correlate with PARPi sensitivity, indicating that a functional HR defect may not be required for response to these agents. A recent study suggests that RS defects may be a better predictive biomarker of CHK1 inhibitor response (13). For doxorubicin and paclitaxel, the overall sensitivities were 45% and 82%, respectively, and also did not correlate with an HR defect. Overall, these data suggest that most organoids derived from sporadic HGSC tumors are HR-proficient and PARPi-resistant.

Correlation of Tumor Mutational Status with Organoid Functional Testing

The low percentage of organoids responding to PARPi (2/22 patients, 9% of patients tested) is surprising, given the high number of patients (up to 50%) hypothesized to have HR-defective tumors by genomic analysis (4, 10). However,

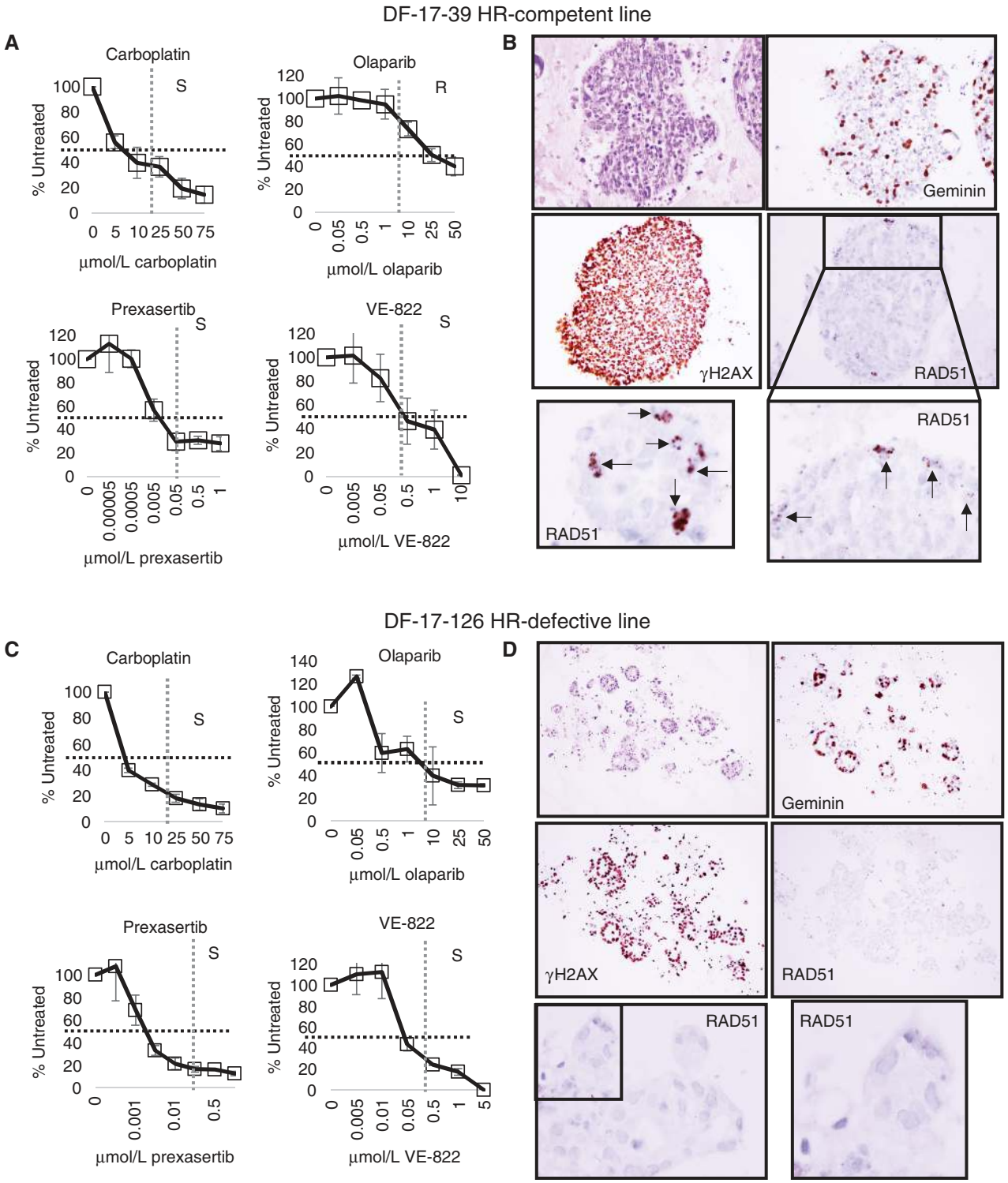

Figure 2. Most HGSC organoids are HR-proficient and lack therapeutic sensitivity to agents targeting HR defects. **A,** Sensitivity dose curves of organoid cultures from one tumor site (transverse colon mesentery) from a *BRCA1* mutation carrier (DF-17-39) with acquired PARPi resistance to carboplatin, olaparib, prexasertib, and VE-822. A dashed black line marks 50% untreated, and a dashed gray line marks our sensitivity standard for this assay for all organoid cultures. S, sensitive; R, resistant. **B,** RAD51 focus formation 4 hours after 10 Gy in DF-17-39 transverse colon mesentery metastasis organoids. Top left, an H&E stain of the organoids; top right, cells in S phase marked by geminin; middle left, DNA damage with γH2AX; middle right, presence of RAD51 foci; bottom, magnified areas of the RAD51 stain. **C,** Sensitivity dose curves of organoid cultures generated from an omental metastasis from an untreated patient with HGSC, DF-17-126, to carboplatin, olaparib, prexasertib, and VE-822. The dose curves are configured as described for **A**. **D,** RAD51 focus formation 4 hours after 10 Gy in DF-17-126. Top left, an H&E stain; top right, cells in S phase marked by geminin; middle left, DNA damage with γH2AX; middle right, a lack of RAD51 foci; bottom, magnified areas of the RAD51 stain.

Table 1. DNA damage repair assay results in the panel of HGSC organoids

Organoid Line	Treatment status	Carbo-platin	Olaparib	Prexa-sertib	VE-822	Doxo-rubicin	Taxol	Gemcit-abine	HU fibers	Prex + carbo fibers	Prex + gem fibers	RAD51 foci	pKAP1/ pCHK1 after prex	Germ-line	Copy-number altera-tion	HRD signa-ture
DF-17-39 Rectosigmoid	Recurrent	S	R	S	S	R	S	S	U	St	U	Yes	Yes	*BRCA1*		Yes
DF-17-39 Transverse colon	Recurrent	S	R	S	S	R	S	S	U	St	U	Yes	Yes	*BRCA1*	*MYC Amp*	Yes
DF-17-39 Supracolic omentum	Recurrent	S	R	S	S	R	S	S	U	St	ND	Yes	Yes	*BRCA1*		Yes
DF-17-39 Diaphragm	Recurrent	S	R	S	S	S	S	S	U	St	ND	Yes	Yes	*BRCA1*		Yes
DF-17-103 Omentum	Neoadjuvant	R	R	R	S	ND	ND	ND	St	ND	ND	Yes	Yes			No
DF-17-104 Omentum	Neoadjuvant	S	R	S	R	ND	ND	ND	U	ND	ND	ND	Yes			No
DF-17-107 Left ovary	Neoadjuvant	R	R	R	R	ND	ND	ND	St	ND	ND	Yes	Yes	*BRCA1*		No
DF-17-107 Right ovary	Neoadjuvant	R	R	S	R	ND	ND	ND	ND	ND	ND	Yes	Yes	*BRCA1*	*MYC Amp*	No
DF-17-107 Omentum	Neoadjuvant	R	R	R	R	ND	ND	ND	ND	ND	ND	ND	Yes	*BRCA1*	*MYC Amp*	No
DF-17-115 Left ovary	Untreated	S	R	S	S	ND	ND	ND	U	ND	ND	ND	Yes	*BRCA2*		Yes
DF-17-116 Omentum	Neoadjuvant	S	R	S	S	S	S	S	U	U	U	Yes	Yes			No
DF-17-121 Pleural effusion	Recurrent	R	R	R	R	R	S	R	St	U	U	Yes	Yes			No
DF-17-123 Right ovary	Untreated	R	R	R	R	ND	ND	ND	U	ND	ND	Yes	Yes			No
DF-17-123 Left ovary	Untreated	R	R	S	S	ND	ND	ND	U	ND	ND	Yes	Yes			No
DF-17-123 Omentum	Untreated	S	R	R	R	ND	ND	ND	U	ND	ND	Yes	Yes		*MYC* Amp	No
DF-17-126 Omentum	Untreated	S	S	S	S	ND	ND	ND	U	ND	ND	No	Yes	*RAD51C*		Yes
DF-17-132 Omentum	Untreated	R	R	R	R	ND	ND	ND	ND	ND	ND	Yes	Yes			No
DF-17-132 Omentum	Neoadjuvant	R	R	R	R	ND	ND	ND	St	ND	ND	Yes	Yes			No
DF-17-132 Cecum	Neoadjuvant	R	R	R	R	ND	ND	ND	St	ND	ND	Yes	Yes			No
DF-17-134 Left ovary	Untreated	S	R	R	R	S	S	S	St	U	U	Yes	Yes			No
DF-17-134 Right ovary	Untreated	R	R	S	S	S	S	S	St	U	U	Yes	Yes			No
DF-18-1 Omentum	Neoadjuvant	R	R	R	R	ND	ND	ND	St	ND	ND	Yes	Yes		*CCNE1* Amp	No
DF-18-7 Right ovary	Untreated	R	R	R	R	ND	ND	ND	U	ND	ND	Yes	Yes			No
DF-18-8 Colonic mesentery	Untreated	S	R	S	S	ND	ND	ND	U	ND	ND	ND	Yes		*MYC* Amp	Weak
DF-18-12 Left ovary	Untreated	R	R	R	R	ND	ND	ND	ND	ND	ND	Yes	Yes		*CCNE1* Amp	No
DF-18-17 Omentum	Neoadjuvant	R	R	R	R	ND	ND	ND	St	ND	ND	Yes	Yes			No
DF-18-23 Right ovary	Neoadjuvant	R	R	R	R	ND	ND	ND	U	ND	ND	No	Yes	*BRCA2*	*MYC* Amp	Yes
DF-18-30 Left ovary	Untreated	S	S	R	S	S	S	S	U	ND	ND	No	Yes	*BRCA2*	*MYC* Amp	Yes
DF-18-43 Omentum	Neoadjuvant	R	R	R	R	ND	ND	ND	ND	ND	ND	Yes	ND			No
DF-18-43 Left ovary	Neoadjuvant	R	R	R	R	ND	ND	ND	St	ND	ND	Yes	Yes			No
DF-18-47 Omentum	Untreated	S	R	S	S	R	R	S	U	ND	ND	Yes	Yes		*CCNE1* Amp	No
DF-18-48 Omentum	Neoadjuvant	R	R	S	S	R	R	R	St	ND	ND	Yes	Yes			No
DF-18-50 Omentum	Neoadjuvant	S	R	S	S	ND	ND	ND	U	ND	ND	Yes	Yes		*CCNE1* Amp	No
DF-18-54 Omentum	Neoadjuvant	R	R	R	R	ND	R	ND	ND	ND	ND	Yes	Yes			No

NOTE: Shown are the patient treatment status at the time of acquisition of tissue for organoid generation, therapeutic sensitivity [for carboplatin, olaparib, prexasertib, VE-822, doxorubicin, paclitaxel (Taxol), and gemcitabine], fork stability after various treatments as indicated by DNA fiber assay results, RAD51 focus formation capability, post-prexasertib western blot results for pKAP1 and pCHK1, HRD signature status, copy-number status, and germline status are shown for all organoid cultures.
Abbreviations: amp, amplification; carbo, carboplatin; gem, gemcitabine; HU, hydroxyurea; ND, not done; prex, prexasertib; R, resistant; S, sensitive; St, stable; U, unstable.

when WES data from tumor–organoid pairs were further evaluated, reasons underlying the low response rate were clarified. We queried multiple aspects of genomic HR markers including somatic mutations, copy-number variation, allelic imbalance, and mutational signatures (Fig. 3; Supplementary Tables S3 and S5).

First, we assessed the parent tumor and organoid WES data for a homologous recombination defect (HRD) mutational signature (26), which is defined by somatic single-nucleotide variants (SNV), as well as insertion–deletion (indel) mutations. This signature is comprised of an elevated rate of both SNVs and deletions, as well as context-specific depletion of C>T substitutions and increased long deletions. This mutational signature was readily detected and quantified in tumors and organoids from 5 of the 6 patients with germline HR gene mutations (DF-17-39, DF-17-115, DF-17-126, DF-18-23, and DF-18-30), weakly detected in a patient with a germline variant of unknown significance in *BRCA1* (DF-18-8), and not detected in sporadic patients (Fig. 3A; Supplementary Table S5). Components of the signature were detected in some sporadic tumors such as DF-18-7, which showed increased long deletions only, or DF-17-123, which weakly demonstrated the signature for SNVs only. Both of these cases with only parts of the HRD signature also lacked PARPi response, suggesting that residual or restored HR was present, that the signature components were associated only with impaired protection of stalled replication forks, or that the observed mutations were due to some other, non-HR, mutational mechanism. We were able to clarify these possibilities with an assay for replication fork stability (see below; Table 1).

The HRD mutational signature was strongest in patient DF-17-126, the patient with a germline mutation in *RAD51C/FANCO*, an ovarian cancer susceptibility gene required for HR repair (27, 28). The DF-17-126 parent tumor and organoid culture had a high number of long deletions and SNVs, consistent with the HRD signature (Fig. 3A; Supplementary Table S5). Examination of the copy-number status of the *RAD51C/FANCO* locus at the site of the patient's known mutation revealed 2 copies and increased allelic imbalance, in favor of the mutant allele (Supplementary Fig. S9A), revealing copy-neutral loss of heterozygosity (LOH) of the wild-type allele in both the parent tumor and organoid culture (Fig. 3B). These genomic data correlated with the olaparib sensitivity and lack of RAD51 foci in the DF-17-126 organoid culture (Fig. 2C and D; Fig. 3B; Supplementary Fig. S9A). Taken together, the genomic HR data combined with the functional data of the organoids strongly predict a functional HR defect in the tumor.

The HRD mutational signature was also strong in DF-18-30, a patient with a germline *BRCA2* mutation who developed a carcinosarcoma (Fig. 3A; Supplementary Table S5). Examination of the copy-number status of the *BRCA2* locus indicated single copy loss and increased allelic imbalance in favor of the mutant allele (Supplementary Fig. S9B), thus revealing LOH of the wild-type allele (Fig. 3C). Again, the genomic data correlated with the olaparib sensitivity and lack of post-IR RAD51 foci in the DF-18-30 organoid culture (Fig. 3C and Table 1). This patient is currently responding to standard-of-care carboplatin/paclitaxel treatment with an ongoing drop in her CA125 (Supplementary Table S4).

In contrast, patient DF-17-107 was a germline carrier of the p.C61G founder mutation in *BRCA1*. A logical prediction is that this patient's tumor arose from LOH of the wild-type *BRCA1* allele and would be olaparib-sensitive. However, the tumor-derived organoids formed RAD51 foci and were olaparib-resistant (Table 1), indicating that the tumor was HR-proficient. Tumor–organoid pairs from this patient did not exhibit an HRD signature (Fig. 3A; Supplementary Table S5). Copy-number interpretation of this patient's samples was impaired by low tumor purity. Reexamination of the germline variant at the *BRCA1* locus in the tumor and organoid lines revealed that only the left ovarian tumor site had mild allelic imbalance and 2 copies, suggesting at least clonal or subclonal copy-neutral LOH in favor of the mutant allele, whereas the right ovary mass and omental metastasis did not exhibit loss of the wild-type allele (Supplementary Figs. S3 and S9C). Taken together, these results suggest that all tumor sites likely express some wild-type BRCA1 (Fig. 3D). These findings are consistent with the functional assay results and absent HRD signature (Table 1). *BRCA1* mutation carriers without loss of the wild-type allele and with intact HR, based on genomic analysis, have been observed previously (29). In addition, the p.C61G mutation has been shown to be sufficient for tumorigenesis but not for platinum or PARPi sensitivity, suggesting that even in the absence of wild-type protein expression, this hypomorph may have functional DNA repair activity (30).

The PARPi-resistant *BRCA1* mutation carrier (DF-17-39) profiled in Fig. 2A and B exhibited the HRD signature, but the magnitude was lower than that observed for DF-17-126 (Fig. 3A; Supplementary Table S5). Each of the tumors and organoids from this patient demonstrated a single copy loss and increased allelic imbalance in favor of the mutant variant of *BRCA1* (Supplementary Fig. S9D), consistent with LOH and rendering the tumor *BRCA1*-deficient (Fig. 3E). However, at the time of organoid generation, the patient was clinically resistant to olaparib (Supplementary Table S4), and the organoid cultures were olaparib-resistant and competent for RAD51 focus formation (Fig. 2A and B; Table 1). No genetic cause for the evolution of the PARPi resistance was discovered. Thus, although genetic analysis suggested that the tumor was HR defective, the organoid functional assays and clinical response revealed that the tumor was PARPi-resistant.

The *BRCA2* germline mutation carrier (DF-17-115) also exhibited the HRD signature (Fig. 3A; Table 1; Supplementary Table S5). The parent tumor and organoid cultures showed single copy loss and increased allelic imbalance in favor of the mutant germline variant in the *BRCA2* locus (Supplementary Fig. S9E), consistent with LOH of the wild-type allele (Fig. 3F). Current treatment selection protocols assume that this would result in an HR-defective, PARPi-sensitive tumor. However, these organoids were PARPi-resistant but carboplatin-, prexasertib-, and VE-822-sensitive, suggesting that the mechanistic defect conferred by this *BRCA2* mutation was a stalled fork protection defect and not an HR defect. These results further support the need for a combined genetic and functional assay approach to targeted therapy selection.

Finally, the tumor from the neoadjuvantly treated *BRCA2* germline mutation carrier (DF-18-23) also exhibited the HRD signature (Fig. 3A; Table 1; Supplementary Table S5). The

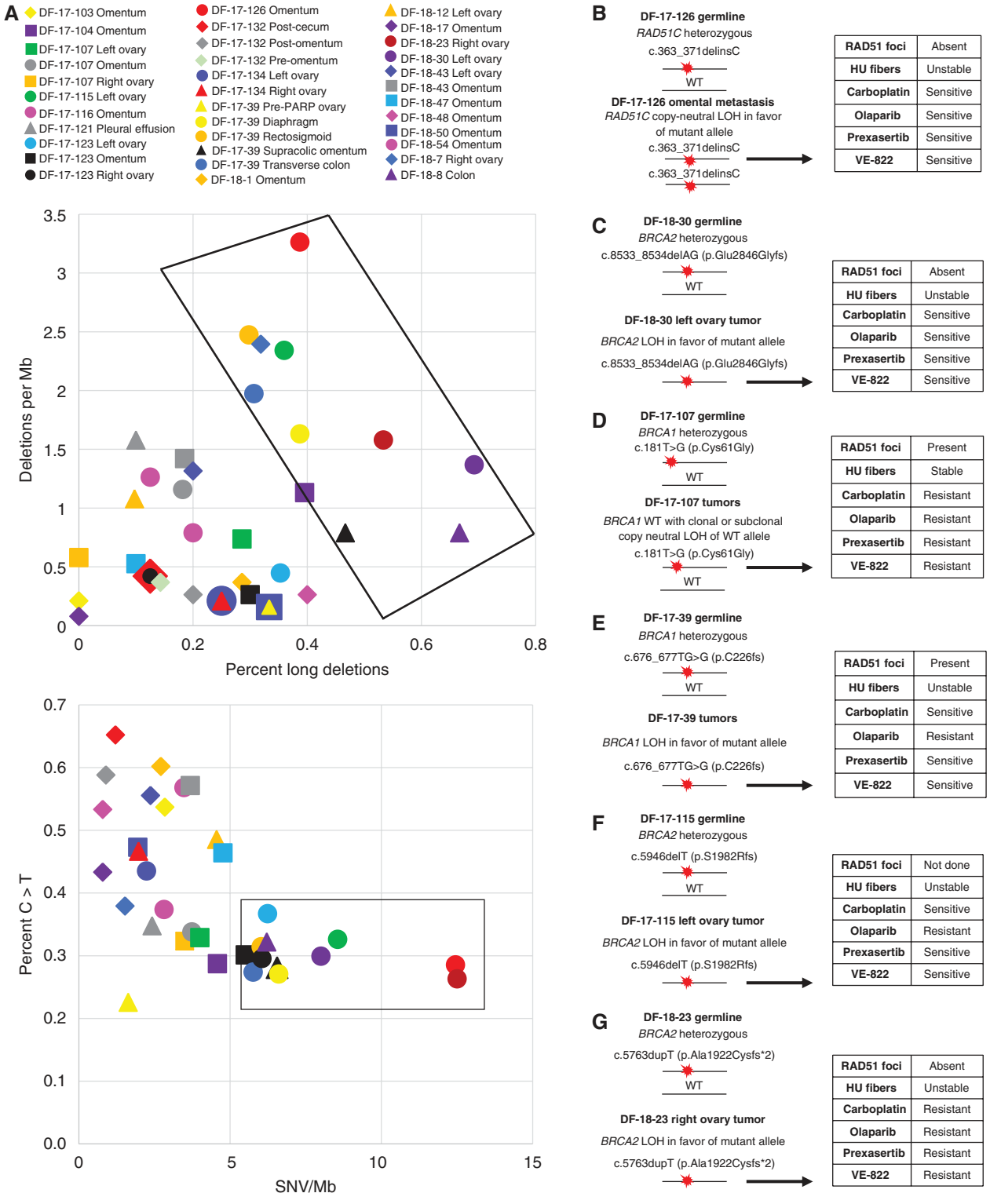

RAD51 foci	Absent
HU fibers	Unstable
Carboplatin	Sensitive
Olaparib	Sensitive
Prexasertib	Sensitive
VE-822	Sensitive

RAD51 foci	Absent
HU fibers	Unstable
Carboplatin	Sensitive
Olaparib	Sensitive
Prexasertib	Sensitive
VE-822	Sensitive

RAD51 foci	Present
HU fibers	Stable
Carboplatin	Resistant
Olaparib	Resistant
Prexasertib	Resistant
VE-822	Resistant

RAD51 foci	Present
HU fibers	Unstable
Carboplatin	Sensitive
Olaparib	Resistant
Prexasertib	Sensitive
VE-822	Sensitive

RAD51 foci	Not done
HU fibers	Unstable
Carboplatin	Sensitive
Olaparib	Resistant
Prexasertib	Sensitive
VE-822	Sensitive

RAD51 foci	Absent
HU fibers	Unstable
Carboplatin	Resistant
Olaparib	Resistant
Prexasertib	Resistant
VE-822	Resistant

Figure 3. Mutational signatures and repair gene mutation status in tumors and organoid cultures. **A,** WES data from parent tumors and organoid cultures were analyzed for numbers of SNVs and long deletions to assess for HRD mutational signatures. Deletions per megabase (Mb) compared with fraction of deletions 5-bp or longer (top) and fraction of C to T substitutions (C > T) and SNVs per Mb (bottom) for each parent tumor and organoid culture are shown for all 34 patients. The organoids and parent tumors harboring components of the HRD mutational signature have a black box enclosing them in each panel. A color code for each patient is at the top of the panels. **B–G,** Germline and tumor allele mutation status and repair assay status for **B,** *RAD51C/FANCO* for DF-17-126; **C,** *BRCA2* for patient DF-18-30; **D,** *BRCA1* for patient DF-17-107; **E,** *BRCA1* for patient DF-17-39; **F,** *BRCA2* for patient DF-17-115; **G,** *BRCA2* for patient DF-18-23.

parent tumor and organoid cultures showed single copy loss and increased allelic imbalance in favor of the mutant germline variant in the *BRCA2* locus (Supplementary Fig. S9F), consistent with LOH of the wild-type allele (Fig. 3G). Current treatment selection protocols predict an HR-defective, PARPi-sensitive tumor. However, these organoids were resistant to PARPi, carboplatin, prexasertib, and VE-822, although they lacked RAD51 foci. This case is particularly interesting clinically. The patient had a protracted treatment course with sporadic periods on and off chemotherapy (Supplementary Table S4). After neoadjuvant chemotherapy, the patient delayed surgery for 7 months, at which time her tumor markers rose and imaging revealed an expanding pelvic mass (Supplementary Table S4). Organoids were established from this pelvic mass at the time of her interval debulking. Taken together, these clinical data suggest that this site was likely selected for therapy resistance through an unknown mechanism. These results further support the need for a combined genetic and functional approach to targeted therapy.

Organoids generated from the tumor from patient DF-18-8 showed a very weak HRD signature (Fig. 3). These organoids were sensitive to carboplatin, prexasertib, and VE-822 but resistant to olaparib. The patient carries a germline variant of unknown significance (VUS) mutation in *BRCA1* (c.4550T>C). Examination of the *BRCA1* locus at the site of the patient's known mutation revealed two copies and increased allelic imbalance, in favor of the mutant allele (Supplementary Fig. S9G). These results reveal copy-neutral LOH of the wild-type allele in both the parent tumor and organoid culture. However, given that the HRD signature was weak, the tumor had high baseline copy-number variation, and the culture was PARPi-resistant, the VUS may be functional, highlighting the importance of the functional assays.

Taken together, these cases explain the PARPi insensitivity of 10 of the 32 resistant organoids in our sample set. To understand the basis of the other 22 resistant organoids, we examined the WES data for somatic mutations or copy-number alterations. No obvious mutations or alterations in HR pathway genes were found (Supplementary Table S3), suggesting that these organoids would be expected to be resistant. Organoids with somatic mutations in *BRCA* pathway genes (for example, the DF-17-104 tumor harboring a *RAD51C* somatic mutation) were identified with a partial HRD signature (Fig. 3A); however, ultimately this line was PARPi-resistant, showing that a functional assay is more predictive than a single somatic mutation.

Although the low rate of PARPi sensitivity is surprising, our results are more accurate than genetic predictions alone. Clinical trials have suggested that some "sporadic" HGSC cases have PARPi response (31, 32); however, the stronger responses occur mostly in *BRCA* or other repair gene mutation carriers with monotherapy (8, 33) or in combination with other therapies (34, 35). Even many of these patients do not respond (31, 32, 36). Larger ongoing trials will determine the response rate in true sporadic patients (37). Still, the organoids in our study functionally match their genomic status and, in the cases where clinical data are available (DF-17-39 and DF-17-121), also match the clinical lack of response (Supplementary Table S4).

WES data combined with the functional assays suggest that even if a patient harbors a germline mutation in an HR gene and exhibits copy-number loss of the wild-type allele or an HRD mutational signature, the tumor cells may not be sensitive to therapies predicted by the mutation (38). The magnitude of the HRD signature reflects the history of a functional defect in a tumor. The most accurate assessment of current defects requires functional assays combined with the germline and somatic genomic data.

Replication Fork Instability Correlates with Sensitivity to Agents Targeting Fork Protection Defects

BRCA1 and BRCA2 have additional roles in the protection of stalled replication forks, discrete from their functions in HR (11, 24, 25, 39). We next tested the organoids for their ability to protect stalled replication forks, using the DNA fiber assay (40). Organoids were sequentially pulsed for equal time periods with two nucleotide analogues, CldU and IdU, followed by exposure to the fork stalling agent hydroxyurea (HU). If the ratio of the track lengths was one, then the fork was protected during replication stalling. If the ratio of the track lengths was less than one, then the fiber containing the second analogue was degraded, indicating that the tumor cell was unable to protect its stalled forks.

Each organoid culture was analyzed by the fiber assay. The organoids were also tested for sensitivity to the fork stalling agent carboplatin, a first-line chemotherapeutic agent for HGSC (Fig. 4; Table 1; ref. 3), as well as for sensitivity to prexasertib and VE-822, in parallel with olaparib. In some cases, other chemotherapy agents, including gemcitabine, paclitaxel, and doxorubicin, were examined. HU and other drug treatments were validated in the fiber assay in OVCAR8 cells (Supplementary Fig. S4B and S4C).

As an example of a tumor with a defect in stalled fork protection, we show the organoid analysis of a sporadic HGSC patient (DF-17-116). These organoids were sensitive to all therapeutic agents tested, except for olaparib, and had an average fiber track length ratio of less than one over three biological replicates (Fig. 4A), consistent with unprotected (unstable) forks. Of note, the culture demonstrated RAD51 focus formation, consistent with the olaparib resistance. In contrast, the organoid analysis of another sporadic HGSC patient (DF-17-132), after neoadjuvant treatment, provides an example of a tumor that is competent for stalled fork protection. This organoid culture was resistant to all four agents and had a fiber track length ratio averaging one (Fig. 4B), consistent with fork stability and functional fork protection. This culture was also positive for RAD51 foci.

Although olaparib sensitivity correlates with the absence of RAD51 focus formation, we hypothesized that sensitivity to the other agents correlates with impaired replication fork protection (i.e., replication fork instability). Indeed, carboplatin sensitivity was associated with fork instability, and carboplatin resistance was associated with fork stability in our organoid panel (Table 1). Seventeen of 28 (61%) organoid cultures tested exhibited unstable forks, suggesting that this mechanistic defect is more common regardless of genomic status. Of the 17 fork-unstable lines tested for drug sensitivity,

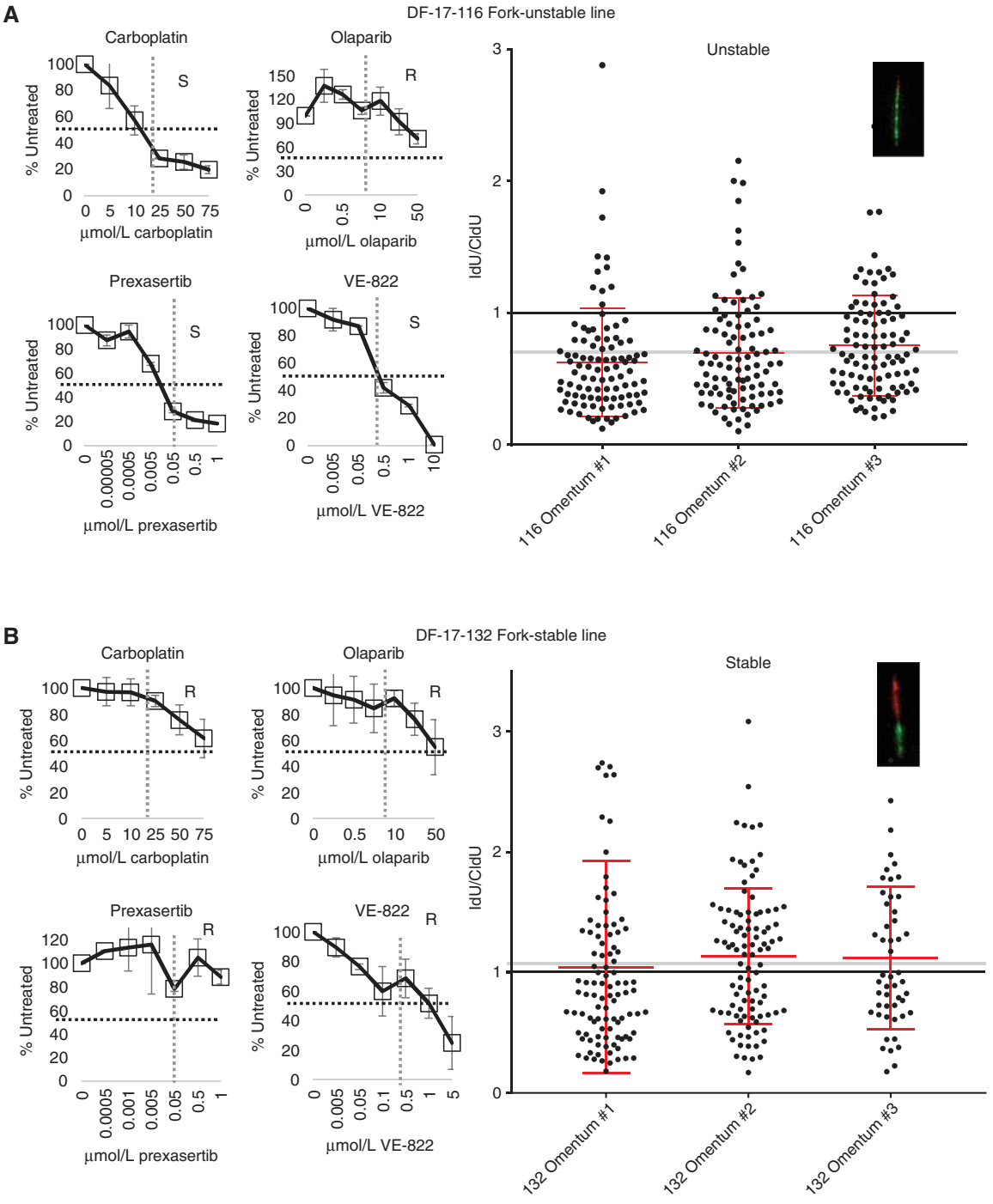

Figure 4. Replication fork stability correlates with carboplatin sensitivity in HGSC organoids. **A,** Sensitivity dose curves (left) and fiber assay results (right) of omental metastasis organoid cultures from a patient with sporadic HGSC (DF-17-116). Dose curves for carboplatin, olaparib, prexasertib, and VE-822 show sensitivity compared with the untreated control. S, sensitive; R, resistant. A dashed black line marks 50% untreated and a dashed gray line marks the sensitivity cutoff for all organoid cultures. On the right, the ratio of IdU to CldU in three biological replicates is shown for DF-17-116 organoids treated with hydroxyurea. A black line marks a ratio of 1, and a gray line marks the average ratio for this line. At the top of the panel is a representative fiber from this line denoting an unstable fork. **B,** Sensitivity dose curves (left) and fiber assay results (right) of organoid cultures from a patient with sporadic HGSC post-neoadjuvant chemotherapy (DF-17-132). Dose curves for carboplatin, olaparib, prexasertib, and VE-822 show sensitivity compared with the untreated control. The graphs are designed as described in **A**. On the right, the ratio of IdU to CldU in three biological replicates is shown for organoids treated with hydroxyurea. A black line marks a ratio of 1, and a gray line marks the average ratio for this line. At the top of the panel is a representative fiber from this line denoting a stable fork.

13 were carboplatin-sensitive (76%). In contrast, 10 of 11 organoids (91%) with stable forks were carboplatin-resistant.

Replication fork instability was associated with sensitivity to prexasertib, VE-822, and possibly gemcitabine. Twelve of the 17 (71%) fork-unstable cultures were prexasertib-sensitive and 9 of the 11 (82%) cultures with stable forks were prexasertib-resistant. Similarly, 12 of the 17 (71%) fork-unstable cultures were VE-822–sensitive and 8 of the 11 (73%) cultures with stable forks were VE-822–resistant. Thus, sensitivity to prexasertib or VE-822 may be associated with replication fork instability as determined by the DNA fiber assay. Finally, 7 of the fork-unstable cultures were tested for gemcitabine sensitivity, and all 7 (100%) were sensitive whereas 2 of the 4 (50%) fork-stable cultures were resistant.

In contrast to the results with carboplatin, prexasertib, VE-822, and gemcitabine, for olaparib, only 2 of the 17 cultures (12%) with unstable forks were sensitive. Although all 11 (100%) of the fork-stable cultures were olaparib-resistant, these cultures were also positive for RAD51 focus formation. Taken together, these data suggest that olaparib sensitivity does not associate with fork instability. Eleven lines were tested for sensitivity to doxorubicin and 12 for paclitaxel, only 7 of which had unstable forks. For doxorubicin, 3 of 7 (43%) fork-unstable lines were sensitive, and for paclitaxel, 6 of 7 (86%) fork-unstable lines were sensitive. Other determinants may govern sensitivity to these agents as well.

Replication fork stability may therefore be a predicator of response or resistance to specific DNA-repair agents. Larger numbers of patient-derived organoids generated from patients treated with the drugs of interest, along with fiber assay analysis, will be required to more accurately measure the predictive power of this assay. The 5 tumor/organoid pairs from patients with germline HR gene mutations and an HRD signature had unstable forks; however, some tumor/organoid pairs from patients with no germline mutation and no HRD signature also had unstable forks, further suggesting diverse mechanisms of fork protection not necessarily linked to HR (Fig. 3; Table 1).

Tumor samples for organoid generation were obtained from 2 patients who underwent laparoscopic biopsy prior to neoadjuvant chemotherapy. For the first patient, DF-17-132, at initial laparoscopic biopsy, the tumor was deemed unresectable, and after neoadjuvant treatment, the patient had only a minimal response to chemotherapy (Supplementary Table S4). Organoids generated from pre- and post-neoadjuvant treatment tumor samples exhibited RAD51 foci, stable replication forks in the case of the post-neoadjuvant samples, and resistance to the four agents tested, consistent with the carboplatin resistance of this patient in the clinic (Fig. 4B; Table 1; Supplementary Table S4). For a second patient who underwent laparoscopic biopsy and neoadjuvant chemotherapy prior to organoid generation, DF-18-47, the tumor was also deemed unresectable at the time of laparoscopic biopsy (Supplementary Table S4). In contrast to patient DF-17-132, however, the tumor-derived organoids from the pretreatment biopsy showed extreme sensitivity to carboplatin, prexasertib, and VE-822, but resistance to olaparib, and demonstrated unstable forks and RAD51 foci (Table 1). At the time of her interval debulking, the patient had minimal tumor tissue, insufficient for the generation of organoids. Her chemotherapy response was therefore predicted by the organoid culture results (Supplementary Table S4). Taken together, these cases indicate that organoid functional and therapeutic studies may be predictive of carboplatin resistance and could be used for window-of-opportunity studies in clinical trials for predicting response to other neoadjuvant agents.

Combined Prexasertib-Mediated Inhibition of CHK1 with Carboplatin or Gemcitabine Promotes Fork Instability

Prexasertib monotherapy is effective for some patients with sporadic HGSCs, consistent with our sporadic organoid culture results (Table 1; ref. 13). Indeed, 12 of the 17 fork-unstable organoids (71%) were prexasertib-sensitive, whereas fork-stable organoids tended to be prexasertib-resistant (Table 1). These results suggest that prexasertib-monotherapy may not be appropriate for all patients and highlight the need for assays to understand functional defects that confer prexasertib sensitivity.

Western blot analysis of 33 of the organoid cultures showed that prexasertib increased DNA damage, indicated by increased expression of γH2AX, and increased RS, as indicated by increased phosphorylated RPA (pRPA). Prexasertib activates the ATR pathway in both fork-unstable and fork-stable lines, as shown by the increased phosphorylation of the ATR targets KAP1 (pKAP1) and CHK1 (pCHK1; Fig. 5A; Table 1; refs. 41, 42). The elevated pCHK1 level is a pharmacodynamic marker of CHK1 inhibition by prexasertib. Prexasertib primes a tumor for sensitivity to other DNA-repair agents by blocking the ATR/CHK1 pathway, thereby increasing RS (12, 41). We reasoned that other agents that amplify RS might synergize with prexasertib and promote fork instability and tumor cell death.

To test this hypothesis, we treated fork-stable or fork-unstable organoids with a combination of prexasertib plus an RS-inducing drug, such as carboplatin or gemcitabine. By western analysis of the RS biomarkers pRPA and pKAP1, prexasertib alone induced significant RS, whereas carboplatin and gemcitabine alone induced minimal RS (Fig. 5A). The prexasertib + carboplatin combination led to similar levels of RS in both fork-stable and fork-unstable lines, compared with prexasertib alone. Interestingly, the prexasertib + gemcitabine combination led to increased RS and ATR activation, compared with either agent alone, in both the fork-stable and fork-unstable lines (Fig. 5A).

In organoids with stable forks, such as the DF-17-134 left ovary cultures, prexasertib, carboplatin, and gemcitabine alone did not destabilize replication forks, as shown by the DNA fiber assay (Fig. 5B; Table 1); however, the combination of prexasertib + carboplatin or prexasertib + gemcitabine enhanced fork instability in these organoids (Fig. 5B). The enhanced destabilization of the replication fork by these drug combinations was also evident in other fork-stable organoids (DF-17-134 right ovary and DF-17-121) and in fork-unstable organoids (DF-17-116; Table 1). In contrast, for fork-unstable organoids that had acquired PARPi resistance (DF-17-39), the prexasertib + gemcitabine combination induced fork instability whereas the prexasertib + carboplatin combination did not (Table 1).

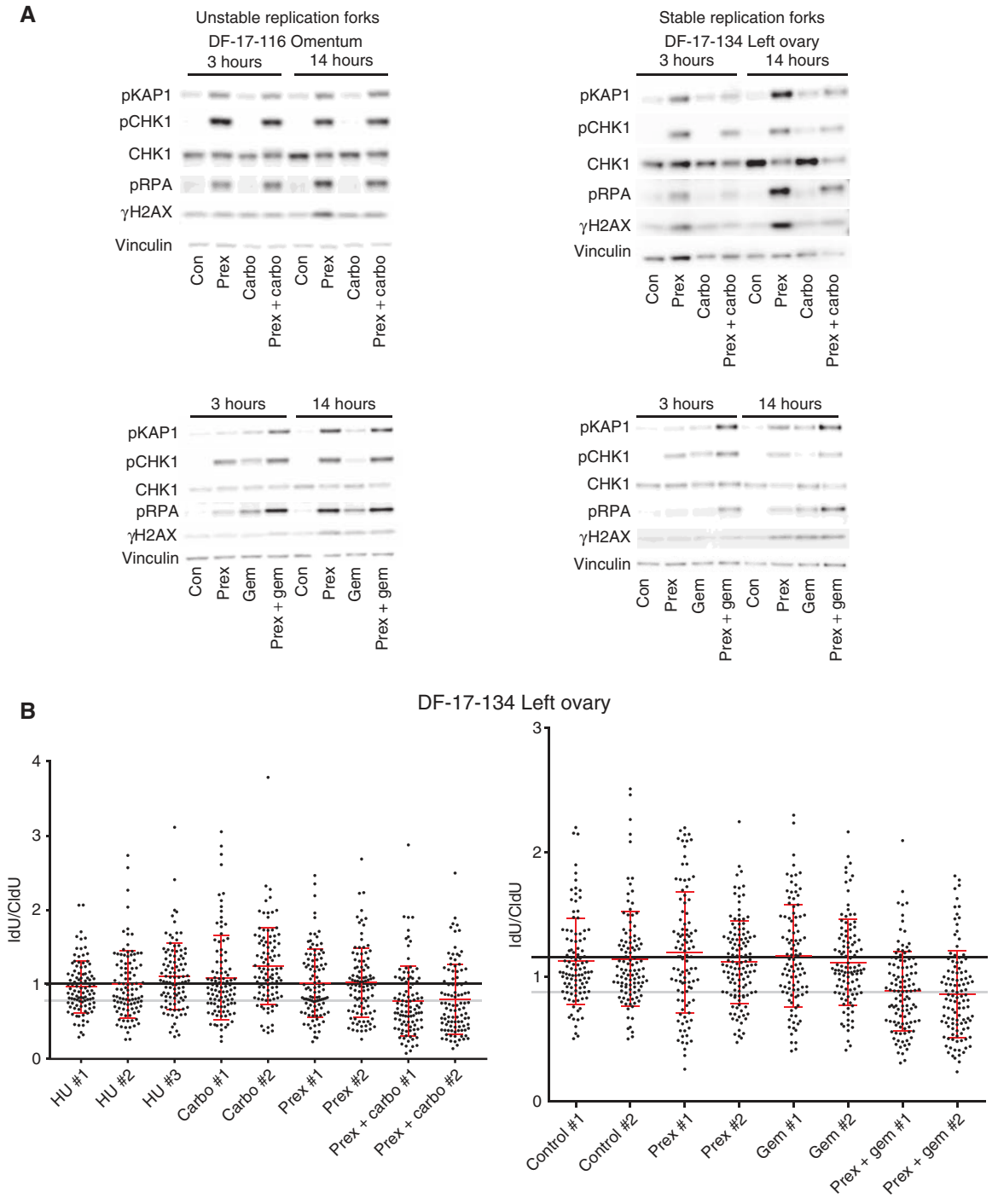

Figure 5. CHK1 inhibitors cause DNA damage in both sporadic and familial HGSCs and confer fork instability in the setting of carboplatin or gemcitabine treatment. **A,** Western blots examining DNA damage in one replication fork-unstable and one fork-stable organoid line. Lines were treated with control (con) media with no drug or media containing in the top plots the CHK1 inhibitor prexasertib (prex) alone, carboplatin (carbo) alone, or prexasertib + carboplatin for either 3 hours or 14 hours; or in the bottom plots with media containing no drug (con), prexasertib alone, gemcitabine (gem) alone, or prexasertib + gemcitabine for either 3 or 14 hours and then harvested for western blot analysis. DNA damage was queried by western blot for phosphorylated KAP1 (pKAP1), phosphorylated RPA (pRPA), and γH2AX. CHK1 expression and DNA damage–induced phosphorylation are also shown. Vinculin is used as a loading control. **B,** Biological replicates of the fiber assay for fork stability in a line with stable forks (DF-17-134 left ovary). Left, the first three replicates show testing of the line using standard hydroxyurea (HU) alone. Next to the HU replicates are two replicates each of the line treated with carboplatin (carbo) alone, prexasertib (prex) alone, and a combination of prexasertib and carboplatin. Right, two replicates each of the line treated with control media with no drug, prexasertib (prex) alone, gemcitabine (gem) alone, or prexasertib + gemcitabine. For the prex, carbo, prex + carbo, prex, gem, and prex + gem experiments, there is no HU in the media at any step, meaning that any fork instability observed is the result of the single drug or drug combination. A black line marks the average stable ratio, and a gray line marks the average of the prexasertib + carboplatin or prexasertib + gemcitabine biological replicates.

These results provide a rationale for treating HGSC with prexasertib in combination with other conventional RS-enhancing agents such as carboplatin and gemcitabine. The fact that the prexasertib + carboplatin combination does not work well for all fork-stable tumors highlights the importance of functional assays in deciphering targetable functional defects. Taken together, these data suggest that proper DNA damage repair drug combinations can be effective in tumors without underlying DNA-repair defects. Short-term organoids are a useful model for rapidly testing these combinations.

DNA Repair Mutation and Gene Copy-Number Analysis Correlates with Organoid Functional Profiling

Genetic alterations in tumors and organoid cultures may lead to fork instability and to varied therapeutic sensitivity patterns. To search for such alterations, we queried the WES data from the parent tumors and corresponding organoids for somatic mutations or copy-number alterations in DNA-repair genes and in other candidate genes derived from The Cancer Genome Atlas (TCGA) ovarian cancer data set. We compared the tumor genome with the germline genome by subtracting out germline mutations and copy-number alterations.

Not surprisingly, 91% of the tumors and organoids from patients with HGSC (30/33 patients) had a mutation in *TP53*, which is almost identical to the 96% observed in the TCGA ovarian cancer data set (Fig. 6; ref. 4). The slightly decreased number of *TP53* mutations detected in our data set could be explained by the fact that we did not test for epigenetic silencing of *TP53* (4). Apart from *TP53* and known germline mutations already described, we did not detect functionally relevant somatic mutations in specific DNA-repair genes, such as *BRCA1/2*, in any of the 34 parent tumors or organoids that could account for the observed fork protection defects (Fig. 6; Supplementary Table S3). These results are consistent with the low somatic mutation burden previously documented in this tumor type (4).

Significant copy-number alterations were evident, consistent with the known high copy-number variation in this disease (4). Indeed, there were deletions observed in many DNA-repair genes involved in both HR and stalled fork repair, including *ATR, FANCD2*, and *RAD51C* (Fig. 6). Given the lack of a functional DNA-repair defects in the organoids (Figs. 1–5; Table 1), it is likely that these alterations do not affect HR or fork protection functions.

We also observed amplifications in Cyclin E1 (*CCNE1*) and *MYC*, known to promote drug resistance in many ovarian tumors (4, 43–45). Four of the 23 patients had *CCNE1*-amplified tumors (DF-18-1, DF-18-12, DF-18-47, and DF-18-50), and 6 of the 23 patients had *MYC*-amplified tumors (DF-17-123, DF-17-39, DF-17-107, DF-18-8, DF-18-23, and DF-18-30; Fig. 6). Only 2 of the *CCNE1*-amplified tumors, DF-18-1 and DF-18-12, and 3 of the *MYC*-amplified tumors, DF-17-123, DF-17-107, and DF-18-23, exhibited resistance to all agents, as expected for these oncogene amplifications (Table 1). Clinically, only patient DF-18-1 had the poor clinical response typical of this class of tumors (Supplementary Table S4). In contrast, *CCNE1*-amplified organoids from DF-18-47 and DF-18-50, along with *MYC*-amplified organoids from DF-17-39, DF-18-8, and DF-18-30, all showed sensitivity to carboplatin, prexasertib, and VE-822. These patients responded to standard therapy to some extent, suggesting that the *CCNE1* or *MYC* amplifications did not alter therapeutic response in these cases (Supplementary Table S4). The variable responses in the organoids and patients across these 2 groups highlight the importance of functional assays in interpreting the therapeutic relevance of copy-number changes.

DISCUSSION

Positive Attributes of the HGSC Organoid System

Our data suggest that patient-derived organoids are a useful model system for rapid assessment of DNA-repair defects in HGSC and highlight their many advantages. The most striking benefit is the clarification of genomic results by the functional assays. Even in this small data set, the functional results indicate that a *BRCA1/2* or Fanconi anemia pathway mutation is neither necessary nor sufficient for conferring an HR defect and PARPi sensitivity (4, 7, 10, 38). This principle is highlighted by tumors from 2 *BRCA1* (DF-17-107 and DF-17-39) and 2 *BRCA2* (DF-17-115 and DF-18-23) germline mutation carriers (Fig. 3; Table 1). Additionally, an HRD mutational signature in a tumor (DF-17-39, DF-17-115, and DF-18-23) did not indicate that the tumor currently has an HR defect (Fig. 3; Table 1). These findings may be due to reasons that are mechanistically complex. For example, patient DF-17-115 has a germline frameshift *BRCA2* mutation, and her tumor shows LOH for the wild-type allele. However, the frameshift occurs in an exon encoding a central region of the protein and may disrupt specific protein interactions, perhaps with FANCD2 but not with PALB2. A BRCA2 hypomorph may therefore maintain some key protein interactions, required for HR, but not other interactions required for fork protection. This example highlights how different functional defects and sensitivities may result from different mutational sites, further underscoring the need for functional assays in predicting repair defects. In contrast, the patient DF-18-23 had a protracted clinical course prior to surgery, perhaps leading to a distinct drug-resistance mechanism, and accounting for the pan-resistance of the corresponding organoid culture. This example demonstrates that therapeutic testing may yield useful information even when the drug-resistance mechanism is incompletely understood.

The organoid data also highlight how functional assays may predict therapeutic response. For example, regardless of genetic status, a stalled fork protection defect was present in 61% of the organoid lines tested, and this defect was associated with carboplatin, prexasertib, and VE-822 sensitivity (Table 1). In contrast, only 6% of organoid lines tested had a functional HR defect and PARPi sensitivity. Overall, this suggests that stalled fork protection defects are more common than HR defects and have a larger array of specific therapies. Although this observation requires validation in a larger set of patient-derived organoid cultures, it suggests that a simple and rapid functional assay may be useful in predicting carboplatin or other therapeutic sensitivity or resistance. Rapid determination of carboplatin resistance, at the time of initial laparoscopic tumor collection, would mandate newer combination therapies up-front in patient treatment. Many correlations between organoid sensitivity patterns and clinical outcome are clearly observed in Supplementary Table S4.

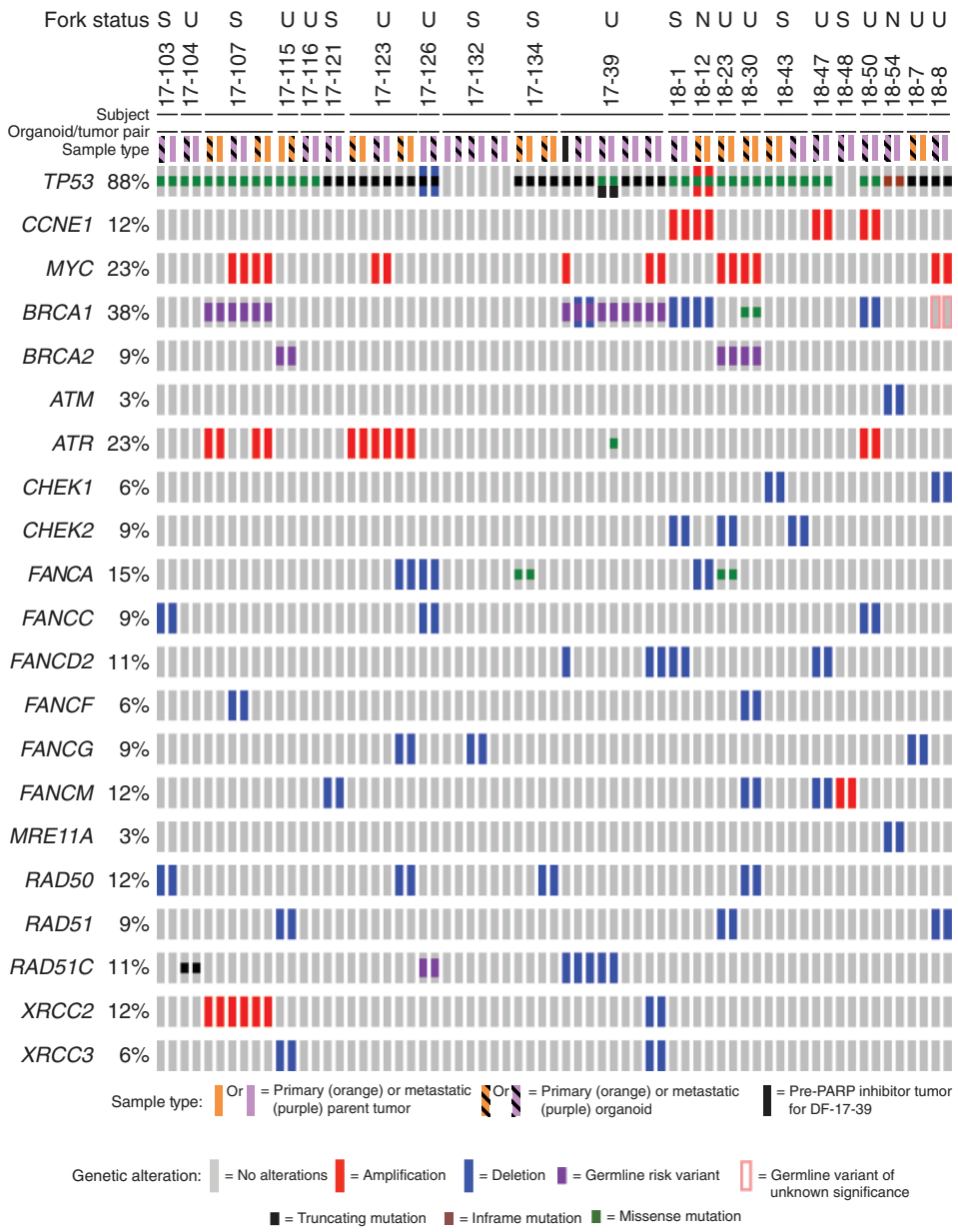

Figure 6. Comparison of somatic mutations and copy-number alterations to fork stability in parent tumor and organoid lines. Somatic mutations and copy-number alterations were identified in parent tumors and organoids. For driver mutations and alterations in DNA-repair genes, there was high concordance of alterations, both between parent tumor and matched organoid, as well as between multiple tumors from the same patient. The full list of somatic alterations can be found in Supplementary Table S3. Shown here are the most relevant DNA repair genes, including *TP53*, *BRCA1*, and *BRCA2*, and the genes with numerous alterations across the data set. The gene is listed on the left, followed by the percentage of tumors or organoids in the data set with an alteration in the gene, followed by the type of alteration in each sample. The samples are listed across the top with a sample and mutation key at the bottom of the figure. For comparison, the fork stability status of the tumor/organoids is at the top of the figure, with the S standing for stable and the U standing for unstable overall. The exact order of the sample pairs from left to right is as follows: DF-17-103-omentum, DF-17-104-omentum, DF-17-107-left ovary, DF-17-107-omentum, DF-17-107-right ovary, DF-17-115-left ovary, DF-17-116-omentum, DF-17-121-pleural effusion, DF-17-123-left ovary, DF-17-123-omentum, DF-17-123-right ovary, DF-17-126-omentum, DF-17-132-post-neoadjuvant cecal mesentery, DF-17-132-post-neoadjuvant omentum, DF-17-132-untreated omentum, DF-17-134-left ovary, DF-17-134-right ovary, DF-17-39-ovary prior to PARPi treatment, DF-17-39-diaphragm, DF-17-39-rectosigmoid mesentery, DF-17-39-supracolic omentum, DF-17-39-transverse colon, DF-18-1-omentum, DF-18-12-left ovary, DF-18-23-right ovary, DF-18-30-left ovary, DF-18-43-left ovary, DF-18-43-omentum, DF-18-47-omentum, DF-18-48-omentum, DF-18-50-omentum, DF-18-54-omentum, DF-18-7-right ovary, and DF-18-8-colonic mesentery.

Human tumors derived from several tissue types exhibit clonal heterogeneity (22, 46), and functional assays in organoids can be used to address the effects of genomic tumor heterogeneity on therapeutic response. We detected multiple examples of tumor heterogeneity in the same patient. For example, multiple different *TP53* mutations were detected in four tumor sites from patient DF-17-39 (Fig. 6; Supplementary Table S3). Also, 2 tumor sites from patient DF-17-123 were carboplatin-resistant, and 1 site was carboplatin-sensitive (Table 1). Functional analyses on organoids from multiple tumor sites will uncover tumor heterogeneity and inform the use of drug combination therapies. Moreover, organoids may be useful in studying different mechanisms by which fork protection defects arise, how to induce these defects, and how best to exploit them for therapeutic benefit.

Furthermore, organoids can be a useful tool in choosing rational drug combinations. Accordingly, combining prexasertib with carboplatin or gemcitabine can enhance replication stress and can destabilize replication forks, even in fork-stable tumors (Fig. 5). Organoids may be useful in rapidly predicting the synergy or antagonism of drug combinations in clinical trials and in identifying rational drug-delivery schedules.

Overcoming Pitfalls of the Organoid Models

Results from other tumor types have raised concerns about organoid models. First, the variable time required for the generation of organoid lines in culture may lead to *in vitro* selection of specific tumor clones (14–16). Second, the large number of growth factors added to the organoid media may lead to epigenetic changes and clonal selection. HGSC organoids grew within 7 to 10 days of plating, and our experiments were performed within 1 to 2 passages of the organoids and within 1 to 2 weeks of tissue collection, mitigating the issues of selection over time. WES analysis was performed on organoid cultures during this timeframe, and the organoids did not accumulate somatic mutations. Also, early cultures did not lose any of the major driver somatic alterations in the tumors (Supplementary Figs. S2 and S3; Supplementary Tables S2 and S3), indicating that the cultures maintained the heterogeneity of the parent tumors. Additionally, although ovarian organoid cultures contain a minimal stromal component and do not faithfully mimic all components of the tumor microenvironment, organoids do contain immune cells (20), and may be useful in studying the immune intereaction with the tumor in real time. Therefore, these cultures may help understand how best to utilize immuno-oncologic agents.

Clinical Implications

Overall, organoids appear to be a useful model of HGSC in which to carry out rapid functional assessment of tumors. In many cases, the drug response of the organoid cultures correlated well with the clinical response of the corresponding patient. The patients in our cohort fall into three clinical groups. The first group consisted of patients presenting with undiagnosed pelvic masses found to be HGSC. We generated organoids from these untreated tumors and then followed how the patients responded to adjuvant therapy in most cases (DF-17-115, DF-17-123, DF-17-126, DF-17-134, DF-18-7, DF-18-8, and DF-18-12) in addition to neoadjuvant therapy prior to interval debulking in two cases (DF-18-47 and DF-17-132; Supplementary Table S4). Some patients have not completed adjuvant treatment or have just completed it, and not enough time has passed to judge recurrence. In the 2 cases where pre-neoadjuvant tissue was obtained (DF-18-47 and DF-17-132), the pretreatment organoids were accurate in predicting response (Supplementary Table S4). In a case with fork-stable organoids (DF-17-134) with variable drug sensitivities, the tumor is already starting to recur (Supplementary Table S4). In the case of fork-unstable organoid lines with platinum sensitivity (DF-17-115, DF-17-123, and DF-17-126), the tumors have not recurred (Supplementary Table S4).

The second group of patients had interval debulking after neoadjuvant chemotherapy (Supplementary Table S4). For these patients, it is unclear whether organoid fork stability or drug sensitivity correlates with the patient clinical courses. Because we sample only some of the tumor at a few sites, we may be growing only specific clones that underwent selection during chemotherapy. Other clones that we do not test may exhibit different responses to therapy. A failure to respond to neoadjuvant therapy may reflect intrinsic tumor heterogeneity, with some clones being sensitive and some with acquired drug resistance or failure of the drug to reach the tumor. Studying organoids from multiple locations in each tumor site will be a critical future goal in these patients.

Finally, the third group of patients were on clinical trials (DF-17-39 and DF-17-121). For the target lesions assessed in these patients, the organoid cultures accurately predicted resistance to an ATR inhibitor in the case of DF-17-121, and PARPi resistance and prexasertib, carboplatin, and gemcitabine sensitivity in the case of DF-17-39 (Supplementary Table S4).

Several of these cases suggest that HGSC organoids, which grow out in only 7 to 10 days, may provide a practical tool for predicting clinical responses of individual patients and for guiding clinical decisions. Future studies with larger patient numbers and longer outcome tracking will be required to determine whether organoid testing will be a reliable *in vitro* assay for predicting drug response in the clinic.

METHODS

Patient Samples

A cohort of patient samples from patients treated at Brigham and Women's Hospital (BWH) and Dana-Farber Cancer Institute (DFCI) was collected for HGSC short-term organoid generation and subsequent analysis between April 2017 and April 2018. Written informed consent was obtained for all subjects on DFCI Institutional Review Board (IRB)–approved protocol 02-051 or Partners (BWH) IRB-approved protocol 2016P002819 prior to the procedure at which the specimen was obtained. The studies were conducted in accordance with the Belmont Report and U.S. Common Rule and approved by the DFCI and Partners (BWH) IRBs.

Organoid Generation and Culture

Pleural effusion fluid was obtained immediately at the time of thoracentesis and was spun at 1000 RPM to create a cell pellet. The pellet was washed two to three times in red blood cell lysis buffer (BioLegend; catalog number 420301), washed once in basal culture media [Advanced DMEM/F12 (Thermo Fisher 12634028), supplemented with 1% penicillin–streptomycin, 1× Glutamax (Life Technologies; catalog number 35050061), and 1% HEPES (Life Technologies;

catalog number 15630080)], and the cell pellet was allocated for WES, histology, and organoid generation. For solid tumors, the tumor was acquired immediately during the surgery. Some fresh tumor was snap-frozen for later WES or fixed immediately in 10% formalin for later histologic analysis. Remaining tumor tissue was transported to the laboratory in basal culture media. The tumor was diced into approximately 2-mm sections and then crushed with the butt of a syringe. This homogenate was then poured into basal culture media containing Type II Collagenase (Life Technologies; #17101015) at a final concentration of 2.5 mg/mL. The homogenate was shaken at 37°C for no longer than 30 minutes. The homogenate was then diluted 1:1 with basal culture media and filtered through a 70-μm filter (Falcon; catalog number 352350). The cell suspension was then spun at 1000 RPM to create a cell pellet. The pellet was washed with red blood cell lysis buffer two to three times and then washed once with basal culture media.

For general culture, once a pellet of either liquid or solid tumor cells was obtained, the cells were mixed with growth factor–reduced Matrigel (Corning; catalog number CB-40230C), with the final concentration of Matrigel at 75%, and there were approximately 10,000 or more cells/cell groups per 10 μL droplet of Matrigel. The suspension was then rapidly plated into a 48-well plate with 15 μL of suspension per well. Once the Matrigel was solidified, 250 μL of general culture medium was added to each well. General culture medium was composed of Advanced DMEM/F12, supplemented with 1% penicillin–streptomycin, 1× Glutamax, 1% HEPES, 100 ng/mL R-spondin 1 (PeproTech; catalog number 120-38), 100 ng/mL Noggin (PeproTech; catalog number 120-10C), 50 ng/mL EGF (PeproTech; catalog number 100-15), 10 ng/mL FGF-10 (PeproTech; catalog number 100-26), 10 ng/mL FGF2 (PeproTech; catalog number 100-18B), 1× B27 (Life Technologies; catalog number 17504044), 10 mmol/L nicotinamide (Sigma-Aldrich; catalog number N0636), 1.25 mmol/L *N*-acetylcysteine (Sigma-Aldrich; catalog number A9165), 1 μmol/L prostaglandin E2 (R&D Systems; catalog number 2296), 10 μmol/L SB202190 (Sigma-Aldrich; catalog number S7076), and 500 nmol/L A83-01 (Sigma-Aldrich; catalog number SML0788). Y-27632 dihydrochloride (AbMole Bioscience; catalog number M1817) was initially tested in early-passage organoid cultures at a concentration of 10 μmol/L but eventually deemed unnecessary for culture maintenance. Overall tissue digestion and cell plating were similar to those described by Drost and colleagues (14).

WES

Detailed methods of DNA isolation and WES are provided in Supplementary Materials and Methods. Upon sequencing completion, candidate somatic variants were filtered using quality, depth, position, and population frequency thresholds. Mutations were visualized with the cBioPortal OncoPrinter script (47, 48). Copy-number alterations were analyzed with GISTIC2.0 (49).

Accession Number

This study has been deposited in the database of Genotypes and Phenotypes (dbGaP) under accession number phs001685.v1.p1.

Please see Supplementary Materials and Methods for remaining Methods.

Disclosure of Potential Conflicts of Interest

G.I. Shapiro reports receiving commercial research grants from Lilly, Sierra Oncology, and Merck/EMD Serono and is a consultant/advisory board member for Lilly, Sierra Oncology, Merck/EMD Serono, and Pfizer. A.D. D'Andrea reports receiving commercial research grants from Eli Lilly & Company, Sierra Oncology, and EMD Serono and is a consultant/advisory board member for Eli Lilly & Company, Sierra Oncology, and EMD Serono. No potential conflicts of interest were disclosed by the other authors.

Authors' Contributions

Conception and design: S.J. Hill, J.V. Bonventre, A.D. D'Andrea
Development of methodology: S.J. Hill, E.A. Roberts, R. Morizane, B.S. Kochupurakkal, J.V. Bonventre
Acquisition of data (provided animals, acquired and managed patients, provided facilities, etc.): S.J. Hill, E.A. Roberts, N.S. Horowitz, M.G. Muto, M.J. Worley Jr, C.M. Feltmate, C. Yang, R. Morizane, K.T. Do, J.F. Liu, U.A. Matulonis, G.I. Shapiro, R.S. Berkowitz, C.P. Crum
Analysis and interpretation of data (e.g., statistical analysis, biostatistics, computational analysis): S.J. Hill, B. Decker, E.A. Roberts, N.S. Horowitz, H. Nguyen, C. Yang, R. Morizane, B.S. Kochupurakkal, K.T. Do, P.A. Konstantinopoulos, U.A. Matulonis, G.I. Shapiro, A.D. D'Andrea
Writing, review, and/or revision of the manuscript: S.J. Hill, B. Decker, E.A. Roberts, N.S. Horowitz, M.G. Muto, M.J. Worley Jr, C.M. Feltmate, M.R. Nucci, E.M. Swisher, H. Nguyen, R. Morizane, K.T. Do, P.A. Konstantinopoulos, J.F. Liu, U.A. Matulonis, G.I. Shapiro, R.S. Berkowitz, C.P. Crum, A.D. D'Andrea
Administrative, technical, or material support (i.e., reporting or organizing data, constructing databases): S.J. Hill, E.A. Roberts, E.M. Swisher, H. Nguyen, C. Yang, G.I. Shapiro, C.P. Crum
Study supervision: S.J. Hill, E.M. Swisher, R. Morizane, K.T. Do, A.D. D'Andrea

Acknowledgments

We would like to thank the 23 generous patients who donated tissue for this work. This research was supported by a Stand Up To Cancer–Ovarian Cancer Research Fund Alliance–National Ovarian Cancer Coalition Ovarian Cancer Dream Team Translational Research Grant (grant number SU2C-AACR-DT16-15). Stand Up To Cancer (SU2C) is a division of the Entertainment Industry Foundation. Research grants are administered by the American Association for Cancer Research, the Scientific Partner of SU2C. This work was also supported by grants from the U.S. National Institutes of Health (R37HL052725, P01HL048546), the U.S. Department of Defense (BC151331P1), the Leukemia and Lymphoma Society (6237-13), the Breast Cancer Research Foundation, the Richard and Susan Smith Family Foundation, and the Bridge Project, a partnership between the Koch Institute for Integrative Cancer Research at MIT and the Dana-Farber/Harvard Cancer Center (to A.D. D'Andrea). Work on RAD51 staining was supported by a Biomarker Supplement to UM1 CA186709 (G.I. Shapiro and A.D. D'Andrea). We would like to thank Eli Lilly for providing us with the prexasertib used for the experiments in this study.

Received May 3, 2018; revised August 15, 2018; accepted September 5, 2018; published first September 13, 2018.

REFERENCES

1. Force USPST, Grossman DC, Curry SJ, Owens DK, Barry MJ, Davidson KW, et al. Screening for ovarian cancer: us preventive services task force recommendation statement. JAMA 2018;319:588–94.
2. Ramalingam P. Morphologic, immunophenotypic, and molecular features of epithelial ovarian cancer. Oncology (Williston Park) 2016;30:166–76.
3. Narod S. Can advanced-stage ovarian cancer be cured? Nat Rev Clin Oncol 2016;13:255–61.
4. Cancer Genome Atlas Research Network. Integrated genomic analyses of ovarian carcinoma. Nature 2011;474:609–15.
5. Murai J. Targeting DNA repair and replication stress in the treatment of ovarian cancer. Int J Clin Oncol 2017;22:619–28.
6. Ceccaldi R, Sarangi P, D'Andrea AD. The Fanconi anaemia pathway: new players and new functions. Nat Rev Mol Cell Biol 2016;17:337–49.
7. Lord CJ, Ashworth A. PARP inhibitors: synthetic lethality in the clinic. Science 2017;355:1152–8.

8. Liu JF, Konstantinopoulos PA, Matulonis UA. PARP inhibitors in ovarian cancer: current status and future promise. Gynecol Oncol 2014;133:362–9.
9. Jenner ZB, Sood AK, Coleman RL. Evaluation of rucaparib and companion diagnostics in the PARP inhibitor landscape for recurrent ovarian cancer therapy. Future Oncol 2016;12:1439–56.
10. Konstantinopoulos PA, Ceccaldi R, Shapiro GI, D'Andrea AD. Homologous recombination deficiency: exploiting the fundamental vulnerability of ovarian cancer. Cancer Discov 2015;5:1137–54.
11. Rondinelli B, Gogola E, Yucel H, Duarte AA, van de Ven M, van der Sluijs R, et al. EZH2 promotes degradation of stalled replication forks by recruiting MUS81 through histone H3 trimethylation. Nat Cell Biol 2017;19:1371–8.
12. Yazinski SA, Comaills V, Buisson R, Genois MM, Nguyen HD, Ho CK, et al. ATR inhibition disrupts rewired homologous recombination and fork protection pathways in PARP inhibitor-resistant BRCA-deficient cancer cells. Genes Dev 2017;31:318–32.
13. Lee JM, Nair J, Zimmer A, Lipkowitz S, Annunziata CM, Merino MJ, et al. Prexasertib, a cell cycle checkpoint kinase 1 and 2 inhibitor, in BRCA wild-type recurrent high-grade serous ovarian cancer: a first-in-class proof-of-concept phase 2 study. Lancet Oncol 2018;19:207–15.
14. Drost J, Karthaus WR, Gao D, Driehuis E, Sawyers CL, Chen Y, et al. Organoid culture systems for prostate epithelial and cancer tissue. Nat Protoc 2016;11:347–58.
15. Gao D, Vela I, Sboner A, Iaquinta PJ, Karthaus WR, Gopalan A, et al. Organoid cultures derived from patients with advanced prostate cancer. Cell 2014;159:176–87.
16. Boj SF, Hwang CI, Baker LA, Chio II, Engle DD, Corbo V, et al. Organoid models of human and mouse ductal pancreatic cancer. Cell 2015;160:324–38.
17. Lee SH, Hu W, Matulay JT, Silva MV, Owczarek TB, Kim K, et al. Tumor evolution and drug response in patient-derived organoid models of bladder cancer. Cell 2018;173:515–28 e17.
18. Dutta D, Heo I, Clevers H. Disease modeling in stem cell-derived 3D organoid systems. Trends Mol Med 2017;23:393–410.
19. Drost J, Clevers H. Organoids in cancer research. Nat Rev Cancer 2018;18:407–18.
20. Jenkins RW, Aref AR, Lizotte PH, Ivanova E, Stinson S, Zhou CW, et al. Ex Vivo Profiling of PD-1 blockade using organotypic tumor spheroids. Cancer Discov 2018;8:196–215.
21. Pauli C, Hopkins BD, Prandi D, Shaw R, Fedrizzi T, Sboner A, et al. Personalized in vitro and in vivo cancer models to guide precision medicine. Cancer Discov 2017;7:462–77.
22. Patch AM, Christie EL, Etemadmoghadam D, Garsed DW, George J, Fereday S, et al. Whole-genome characterization of chemoresistant ovarian cancer. Nature 2015;521:489–94.
23. Kochupurakkal BS, Parmar K, Lazaro JB, Unitt C, Shapiro GI. Abstract 2796: development of a RAD51-based assay for determining homologous recombination proficiency and PARP inhibitor sensitivity. 2017; Washington, DC. Cancer Research.
24. Schlacher K, Christ N, Siaud N, Egashira A, Wu H, Jasin M. Double-strand break repair-independent role for BRCA2 in blocking stalled replication fork degradation by MRE11. Cell 2011;145:529–42.
25. Pathania S, Nguyen J, Hill SJ, Scully R, Adelmant GO, Marto JA, et al. BRCA1 is required for postreplication repair after UV-induced DNA damage. Mol Cell 2011;44:235–51.
26. Bignell GR, Greenman CD, Davies H, Butler AP, Edkins S, Andrews JM, et al. Signatures of mutation and selection in the cancer genome. Nature 2010;463:893–8.
27. Somyajit K, Subramanya S, Nagaraju G. Distinct roles of FANCO/RAD51C protein in DNA damage signaling and repair: implications for Fanconi anemia and breast cancer susceptibility. J Biol Chem 2012;287:3366–80.
28. Loveday C, Turnbull C, Ruark E, Xicola RM, Ramsay E, Hughes D, et al. Germline RAD51C mutations confer susceptibility to ovarian cancer. Nat Genet 2012;44:475–6; author reply 6.
29. Maxwell KN, Wubbenhorst B, Wenz BM, De Sloover D, Pluta J, Emery L, et al. BRCA locus-specific loss of heterozygosity in germline BRCA1 and BRCA2 carriers. Nat Commun 2017;8:319.
30. Drost R, Bouwman P, Rottenberg S, Boon U, Schut E, Klarenbeek S, et al. BRCA1 RING function is essential for tumor suppression but dispensable for therapy resistance. Cancer Cell 2011;20:797–809.
31. Gelmon KA, Tischkowitz M, Mackay H, Swenerton K, Robidoux A, Tonkin K, et al. Olaparib in patients with recurrent high-grade serous or poorly differentiated ovarian carcinoma or triple-negative breast cancer: a phase 2, multicentre, open-label, non-randomised study. Lancet Oncol 2011;12:852–61.
32. Sandhu SK, Schelman WR, Wilding G, Moreno V, Baird RD, Miranda S, et al. The poly(ADP-ribose) polymerase inhibitor niraparib (MK4827) in BRCA mutation carriers and patients with sporadic cancer: a phase 1 dose-escalation trial. Lancet Oncol 2013;14:882–92.
33. Ledermann JA, Harter P, Gourley C, Friedlander M, Vergote I, Rustin G, et al. Overall survival in patients with platinum-sensitive recurrent serous ovarian cancer receiving olaparib maintenance monotherapy: an updated analysis from a randomised, placebo-controlled, double-blind, phase 2 trial. Lancet Oncol 2016;17:1579–89.
34. Dean E, Middleton MR, Pwint T, Swaisland H, Carmichael J, Goodege-Kunwar P, et al. Phase I study to assess the safety and tolerability of olaparib in combination with bevacizumab in patients with advanced solid tumours. Br J Cancer 2012;106:468–74.
35. Liu JF, Barry WT, Birrer M, Lee JM, Buckanovich RJ, Fleming GF, et al. Combination cediranib and olaparib versus olaparib alone for women with recurrent platinum-sensitive ovarian cancer: a randomised phase 2 study. Lancet Oncol 2014;15:1207–14.
36. Audeh MW, Carmichael J, Penson RT, Friedlander M, Powell B, Bell-McGuinn KM, et al. Oral poly(ADP-ribose) polymerase inhibitor olaparib in patients with BRCA1 or BRCA2 mutations and recurrent ovarian cancer: a proof-of-concept trial. Lancet 2010;376:245–51.
37. Ledermann JA. First-line treatment of ovarian cancer: questions and controversies to address. Ther Adv Med Oncol 2018;10:1758835918768232.
38. AlHilli MM, Becker MA, Weroha SJ, Flatten KS, Hurley RM, Harrell MI, et al. In vivo anti-tumor activity of the PARP inhibitor niraparib in homologous recombination deficient and proficient ovarian carcinoma. Gynecol Oncol 2016;143:379–88.
39. Ray Chaudhuri A, Callen E, Ding X, Gogola E, Duarte AA, Lee JE, et al. Replication fork stability confers chemoresistance in BRCA-deficient cells. Nature 2016;535:382–7.
40. Nieminuszczy J, Schwab RA, Niedzwiedz W. The DNA fibre technique - tracking helicases at work. Methods 2016;108:92–8.
41. Bryant C, Rawlinson R, Massey AJ. Chk1 inhibition as a novel therapeutic strategy for treating triple-negative breast and ovarian cancers. BMC Cancer 2014;14:570.
42. Saldivar JC, Cortez D, Cimprich KA. The essential kinase ATR: ensuring faithful duplication of a challenging genome. Nat Rev Mol Cell Biol 2017;18:622–36.
43. Torigoe T, Izumi H, Ishiguchi H, Yoshida Y, Tanabe M, Yoshida T, et al. Cisplatin resistance and transcription factors. Curr Med Chem Anticancer Agents 2005;5:15–27.
44. Etemadmoghadam D, Weir BA, Au-Yeung G, Alsop K, Mitchell G, George J, et al. Synthetic lethality between CCNE1 amplification and loss of BRCA1. Proc Natl Acad Sci U S A 2013;110:19489–94.
45. Kroeger PT Jr., Drapkin R. Pathogenesis and heterogeneity of ovarian cancer. Curr Opin Obstet Gynecol 2017;29:26–34.
46. Hunter KW, Amin R, Deasy S, Ha NH, Wakefield L. Genetic insights into the morass of metastatic heterogeneity. Nat Rev Cancer 2018;18:211–23.
47. Gao J, Aksoy BA, Dogrusoz U, Dresdner G, Gross B, Sumer SO, et al. Integrative analysis of complex cancer genomics and clinical profiles using the cBioPortal. Sci Signal 2013;6:pl1.
48. Cerami E, Gao J, Dogrusoz U, Gross BE, Sumer SO, Aksoy BA, et al. The cBio cancer genomics portal: an open platform for exploring multidimensional cancer genomics data. Cancer Discov 2012;2:401–4.
49. Mermel CH, Schumacher SE, Hill B, Meyerson ML, Beroukhim R, Getz G. GISTIC2.0 facilitates sensitive and confident localization of the targets of focal somatic copy-number alteration in human cancers. Genome Biol 2011;12:R41.